Photophysical Analysis and Protein Binding Study of a Novel Synthesized Oxazole Derivative

Dissertation submitted to

Visvesvaraya National Institute of Technology, Nagpur

In partial fulfillment of the requirements for the award of the degree

Master of Science

in

Chemistry

by

Puneet Mishra (MS23CHM012)

under the guidance of

Prof. Sujit Kumar Ghosh

Department of Chemistry

Visvesvaraya National Institute of Technology

Nagpur 440010 (India)

May 2025

Photophysical Analysis and Protein Binding Study of a Novel Synthesized Oxazole Derivative

Dissertation submitted to

Visvesvaraya National Institute of Technology, Nagpur

In partial fulfillment of the requirements for the award of the degree

Master of Science

in

Chemistry

by

Puneet Mishra (MS23CHM012)

under the guidance of

Prof. Sujit Kumar Ghosh

Department of Chemistry

Visvesvaraya National Institute of Technology

Nagpur 440010 (India)

May 2025

© Visvesvaraya National Institute of Technology (VNIT) 2025

Department of Chemistry

Visvesvaraya National Institute of Technology, Nagpur

Declaration

I, **Puneet Mishra** hereby declare that this dissertation titled **"Photophysical Analysis and Protein Binding Study of a Novel Synthesized Oxazole Derivative"** is carried out by me in the Department of Chemistry of Visvesvaraya National Institute of Technology, Nagpur. The work is original and has not been submitted earlier whole or in part for the award of any degree/diploma at this or any other Institution / University.

Puneet Mishra (MS23CHM0012)

Date:

Certificate

This is to certify that the dissertation titled **"Photophysical Analysis and Protien Binding Study of a Novel Synthesized Oxazole Derivative"** is submitted by **Puneet Mishra** in partial fulfilment of the requirements for the award of the degree of **Master of Science in Chemistry, VNIT Nagpur.** The work is comprehensive, complete and fit for final evaluation.

Dr. Sujit Kumar Ghosh

Professor & Head

Department of Chemistry, VNIT Nagpur

Head of the Department

Department of Chemistry

VNIT, Nagpur

Date:

Visvesvaraya National Institute of Technology, Nagpur

Department of Chemistry

Non-Plagiarism Certificate

Certified that M.Sc. dissertation titled **"Photophysical Analysis and Protein Binding Study of a Novel Synthesized Oxazole Derivative"** submitted by **Puneet Mishra** Enrollment No. **MS23CHM012** ID No. 30594 has been checked for plagiarism using TURNITIN software, and the overlap is found within prescribed limits. A summary of the report is given below.

ORIGINALITY REPORT			
24%	13%	20%	8%
SIMILARITY INDEX	INTERNET SOURCES	PUBLICATIONS	STUDENT PAPERS

Puneet Mishra

(MS23CHM0012)

30594

Dr. Sujit Kumar Ghosh

Professor & Head

Department of Chemistry, VNIT Nagpur

Acknowledgment

I would like to express my sincere gratitude to my supervisor, **Prof. Sujit Kumar Ghosh**, for his exceptional guidance, unwavering support, and invaluable mentor ship throughout my journey as a M.Sc. student. I am forever indebted for his remarkable expertise, patience, and dedication in guiding me through conducting research and writing this thesis. Your astute insights, constructive feedback, and visionary guidance have been instrumental in shaping the direction of my work. You have consistently challenged me to think critically, encouraged me to explore new avenues of inquiry, and inspired me to reach for excellence.

I would also like to express my gratitude to **Dr. Kapil Ganorkar** for his guidance and unwavering support throughout my project.

I want to express my special gratitude to all the members of the Photochemistry and Biophysical Spectroscopy Laboratory- Dr. Piyush Singh, Ms. Aditi Garg, Ms. Shrestha Banerjee, Mr. Subham chattopadhyay, Mr. Subham Das, and Ms. Riya Upadhyay who have accompanied me on this academic journey. Your camaraderie, intellectual discussions, and collaborative efforts have enriched my experience in countless ways. Through our shared challenges and triumphs, I have not only grown as a researcher but also formed lasting friendships and a supportive network. Your diverse perspectives, stimulating debates, and willingness to lend a helping hand have been invaluable, and I am grateful for the opportunity to be part of such an inspiring community.

I express my heartfelt gratitude to my parents and family for their constant support, affection, and motivation during this project. Their firm faith in my capabilities and their consistent encouragement provided me with the resilience and resolve to overcome difficult moments. Without their limitless support and unconditional love, this accomplishment would not have been attainable.

Furthermore, I would like to express my heartfelt gratitude to some special persons of my life — Ms. Sakshi Payasi, Mr. Himanshu Mishra, Mr. Sharad Mishra, and Ms.

Nishika Tiwari — whose unwavering support, constant encouragement, and genuine belief in my potential have been a source of strength throughout this journey. Their kind words in moments of doubt, their shared joy in moments of success, and their presence through all the ups and downs have left an indelible mark on my heart. I am truly blessed to have such wonderful souls by my side.

Finally, I want to express my special thanks to **Mr. Subham Chattopadhyay**. Words fall short when it comes to describing what he means to me — his presence alone gives me the strength to face any situation.

Puneet Mishra

DEDICATED TO

MOST DISCIPLINED PERSON I HAVE EVER MET

MR. PRAVEEN MISHRA

Abstract:

Oxazoles are a class of five-membered heterocyclic aromatic compounds containing one oxygen and one nitrogen atom at the 1 and 3 positions, respectively. These heterocycles are of significant interest in both synthetic and medicinal chemistry due to their unique electronic properties and broad biological activities. They are a major class of heterocyclic compounds found in many natural products and synthetic molecules, and they exhibit a wide range of biological activities. The present study summarizes the synthesis, characterization and complete photophysical analysis of an novel oxazole derivative i.e. 2-(4-(diethylamino)-2-hydroxyphenyl)naphtho[1,2-d]oxazole-5-sulfonic acid (RSM) using ^{1}H NMR, UV- Vis absorption spectroscopy, steady state fluorescence spectroscopy and time resolved fluorescence spectroscopy. Complete photophysical analysis in various solvents shows that only charge transfer process is taking place in the excited state of RSM. Considering the biological and medicinal importance of oxazoles, the interaction of RSM with model transport protein bovine serum albumin (BSA) was investigated under physiological conditions by methods of fluorescence spectroscopy, UV-vis absorption, time resolved emission spectroscopy. The in vitro spectroscopic analyasis were corroborated with in silico molecular docking. The fluorescence data showed that the fluorescence quenching of BSA by RSM was the result of primarily ground state with minor contribution of excited state complex formation. Time-resolved emission spectroscopy further confirmed the quenching mechanism. Site marker competitive experiments indicated that the binding of RSM to BSA occurred mainly at Sudlow site I subdomain IIA. Moderate to high association of RSM with BSA encourages an allosteric modulation leading to deformation in its secondary and tertiary structure which can be seen in 3D fluorescence spectra. All these experimental results are consistent with in silico studies. The consolodated spectroscopic research discribed here in may give anormous information about the future use of oxazole derivative for medicinal chemistry research.

S.No.	Title of Figures	Page no.
1	The Jablonski diagram.	2
2	Illustration of the Franck-Condon Principle.	4
3	P-type and E-type delayed fluorescence mechanisms.	7
4	Effect of solvent polarity on n→π* and π →π* transitions.	10
5	Bathochromic, Hypsochromic, Hyperchromic, Hypochromic shifts summarized.	11
6	Jablonski diagram for fluorescence with solvent relaxation.	13
7	Comparison of dynamic and static quenching.	16
8	Synthetic route of RSM.	21
9	The Beer-Lambert Law.	23
10	Optical system diagram of double-beam UV-vis spectrophotometer JASCO V-630.	24
11	Optical system diagram of spectrofluorometer FP-8300	26
12	Liquid Nitrogen Cooling unit of PMU-830 phosphorescence accessory spectrofluorometer FP-8300 used for phosphorescence measurements.	27
13	Condition of shutter and observed signal; F and P represent fluorescence and phosphorescence respectively.	28
14	Relation between [Delay Time], [Display Time] and [ChoppingPeriod] on phosphorescence lifetime measurement.	29
15	Schematic representation of TCSPC.	31
16	Electronics module involved in TCSPC	33
17	^{1}H NMR spectrum of RSM.	37
18	Absorption spectra of RSM (1mM) in various solvents [298 K].	38
19	Excited state molecular orbitals of RSM (A) LUMO (B) HOMO.	39
20	Optimized structure of RSM (A) Ground state (B) Excited state.	40

21	Emission spectra of RSM (1mM mM) in various solvents [298 K].	40
22	Excitation spectra of RSM in various solvents [298 K].	41
23	Emission spectra of RSM in various solvents when excited at around 250nm [298K].	41
24	Lifetime of RSM in Different Solvents.	42
25	Emission spectra of RSM in toluene when excited at around 250nm [298 K].	43
26	Emission spectra of RSM in Glycerol - Methanol solvent system [298 K].	44
27	RSM in different solvents under White Light.	45
28	RSM in different solvents under UV Light.	45
29	Emission spectra showing quenching of BSA tryptophan fluorescence with increasing RSM concentration at 294 K.	47
30	Emission spectra showing quenching of BSA tryptophan fluorescence with increasing RSM concentration at 298 K.	47
31	Emission spectra showing quenching of BSA tryptophan fluorescence with increasing RSM concentration at 304 K.	48
32	Stern–Volmer plots at varying temperatures Depicting the quenching interaction between RSM and BSA.	49
33	Double logarithmic plot for binding affinity between RSM and BSA.	50
34	Modified Stern–Volmer plots at different temperature illustrating the interaction between RSM and BSA.	51
35	Van't Hoff plots illustrating the temperature dependent binding behavior between RSM and BSA.	52
36	Time-Resolved Fluorescence Decay of BSA upon Increasing [RSM] at 298 K. Excitation at 280 nm, Emission at 330 nm, pH 7.4.	54
37	Fluorescence Emission Profiles of BSA with Warfarin and RSM at 298 K.	57
38	Fluorescence Emission profiles of BSA with Ibuprofen and RSM at 298K.	57

39	Modified Stern–Volmer plots illustrating the binding interaction of RSM with BSA in the absence and presence of site-specific probes Ibuprofen and Warfarin at 298 K.	58
40	Time-resolved fluorescence decay of BSA with increasing [Warfarin] at 298 K.	58
41	Fluorescence decay profiles of BSA at 298 K showing Variation with increasing concentrations of Warfarin.	59
42	3D Fluorescence spectra of BSA only.	61
43	3D Fluorescence spectra of RSM- BSA.	61
44	Lowest-energy binding conformation of RSM positioned within the hydrophobic cavity of Sudlow site I (subdomain IIA) of BSA (PDBID: 3VO3).	63
45	2D Interaction Map Depicting Key Residue Contacts Stabilizing RSM within the BSA Binding Pocket	63

S.No.	Title of Tables	Page no.
1	Lifetime Data of RSM in different solvents	42
2	Quenching parameters of RSM-BSA interaction at various temperatures.	49
3	Temperature-Dependent Thermodynamic Parameters for the RSM–BSA System	53
4	Lifetime Data for Varying [RSM] in the Environment of BSA at 298 K, P^H 7.4.	55
5	Parameters of Competitive Site Replacement Experiments at 298 K for RSM Binding to BSA.	56
6	Lifetime Data for varying [Warfarin] in the Environment of BSA at 298 K, P^H 7.4.	59
7	Lifetime Data for Increasing [Ibuprofen] in the BSA Environment at 298 K, P^H 7.4.	60

Abbreviations

1H NMR: Proton Nuclear Magnetic Resonance

2D : Two-Dimensional

3D: Three-Dimensional

A: Acceotor

AO: Acridine Orange

ACQ: Aggregation Caused Quenching

ADC: Analog-to-Digital Converter

AIE: Aggregation Induced Emission

AIEE: Aggregation Induced Enhanced Emission (AIEE)

AIEgen: Aggregation Induced Emission Generator

BSA: Bovine Serum Albumin

CFDs: Constant Fraction Discriminators

CT: Charge Transfer

D: Donor

DMSO : Dimethyl Sulfoxide

DNA : Deoxyribonucleic Acid

DSC : Dye-Sensitized Solar Cell

DAS: Diethylamino salicylaldehyde

EE: Electronic Excitation

ESIPT: Excited State Intramolecular Proton Transfer

F: Fluorescence

FRET: Fluorescence Resonance Energy Transfer

FTIR: Fourier Transform Infrared Spectroscopy

HPLC: High-performance Liquid Chromatography

HOMO: Highest Occupied Molecular Orbital

HAS: Human Serum Albumin

IC: Internal Conversions

ICT: Intramolecular Charge Transfer

IRF: Instrument Response Function

ISC: Intersystem Crossings

LUMO: Lowest Unoccupied Molecular Orbital

MeOH : Methanol

OLEDs: Organic Light Emitting Diodes

OLETs: Organic Light Emitting Transistors

PH: Phosphorescence

QE : Quantum Efficiency

RIM: Restrictions of Intramolecular Motions

RIR: Restrictions of Intramolecular Rotations

RIV: Restrictions of Intramolecular Vibrations

SDS: sodium dodecyl sulphate

SEM: Scanning Electron Microscopy

TAC: Time-to-Amplitude Converter

TCSPC: Time-correlated Single Photon Counting

TICT: Twisted Intramolecular Charge Transfer

TRF: Time-resolved Fluorescence

UV: Ultraviolet

UV-Vis : Ultraviolet-Visible

VR: Vibrational Relaxations

WD: Window Discriminator

.

LIST OF CONTENTS

CHAPTER-1

1.1 Fundamental Principle of Photophysical Processes
1.1.1 Jablonski Diagram
1.1.2 Franck-Condon Principle
1.1.3 Kasha's rule
1.2 Radiative Decay Processes
1.2.1 Fluorescence
1.2.2 Phosphorescence
1.2.3Delayed Fluorescence
1.3 Nonradiative Decay Processes
1.3.1 Vibrational Relaxation
1.3.2 Internal conversion
1.3.3 Intersystem crossing
1.3.4 Reverse Intersystem Crossing
1.4 Solvent and Environmental Effect on Absorption Spectra
1.5 Solvent and Environmental Effect on Emission Spectra
1.5.1 Effects of solvent polarity
1.6 Fluorescence Quenching
1.6.1 Collisional Quenching
1.6.2 Static Quenching
1.7 Introduction
1.8 Aim and objective of the thesis
1.9 Objectives of the work

CHAPTER-2

2.1 Materials
2.2 Synthesis of RSM
2.3 Instrumentation and methodology

2.3.1 UV-vis Spectrophotometer
2.3.2 Spectrofluorometer
2.3.3 Time-resolved fluorescence spectroscopy
2.3.4 Quantum Chemical Calculations of RSM

CHAPTER-3

3.1 Spectral characterization of RSM
3.2 Spectral Analysis of RSM in Different Solvents
3.2.1 UV- Vis Absorption Study of RSM
3.2.2 Steady State Fluorescence Emission Study of RSM
3.2.3 Time Resolved Fluorescence Emission Study of RSM
3.2.4 Concentration Dependent Study of RSM in Toluene
3.2.5 Test for Twisted Intramolecular Charge Transfer in RSM
3.2.6 Naked Eye Visualization of Intramolecular Charge Transfer in RSM
3.3 Elucidating the Binding Mechanism of RSM with Bovine serum Albumin (BSA) Through Spectroscopic and In Silico Approaches
3.3.1 Characterization of the RSM–BSA Interaction and Its Underlying Binding Mechanism
3.3.2. Thermodynamic Analysis of the RSM–BSA Binding Interaction
3.3.3 Dynamics of the Excited State
3.3.4 Identification of RSM binding site in bovine serum albumin protein
3.3.5 3D Fluorescence Spectral Analysis of RSM–BSA Interaction
3.3.6 In Silico Exploration of Amino Acid Residues Near the Binding Site

Chapter 4

4.1 conclusion
4.2 Future plans

Chapter 5

5.1 References

CHAPTER-1
INTRODUCTION AND OVERVIEW

1.1 Fundamental Principle of Photophysical Processes

1.1.1 Jablonski Diagram

The Jablonski diagram is a widely used conceptual tool that illustrates the various photophysical processes a molecule undergoes upon light absorption. Introduced in the 1930s by Polish physicist Aleksander Jablonski, the diagram provides a visual representation of the electronic and vibrational energy levels of a molecule, along with the transitions between these states—both radiative and non-radiative.[1]

In a Jablonski diagram, energy levels are shown as horizontal lines, increasing from bottom to top. These energy levels are organized according to their spin multiplicity, with singlet states (S_0, S_1, S_2, etc.) on one side and triplet states (T_1, T_2, etc.) on the other. The ground state (S_0) represents the lowest energy level where all electrons are paired. Upon absorbing a photon, a molecule can be excited to a higher energy singlet state (e.g., S_1 or S_2) if the electron maintains its spin orientation. If the electron undergoes a spin inversion, the molecule may transition to a triplet state (T_1), which has a different spin configuration and lower probability of returning to the ground state via radiative processes.

Immediately after excitation, the molecule may occupy a higher vibrational level within an excited electronic state. Vibrational relaxation to the lowest vibrational level of the excited state typically occurs in femtoseconds to picoseconds, releasing excess energy as heat. This process is called internal conversion (IC) and is non-radiative.

From the lowest vibrational level of the first excited singlet state (S_1), the molecule can undergo several pathways:

Fluorescence (FP): A radiative transition from S_1 to S_0, resulting in the emission of a photon. This process is spin-allowed and occurs on the nanosecond timescale.[1]

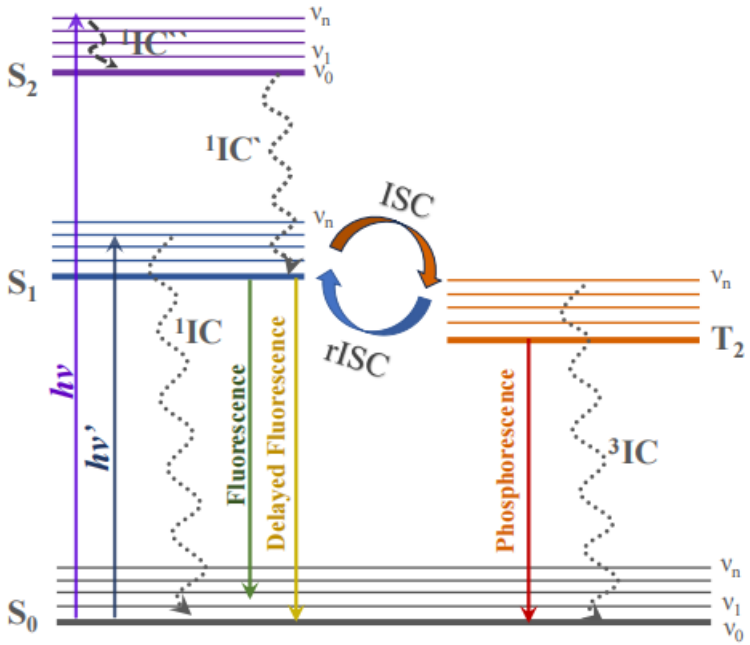

Fig. 1.1 : The Jablonski diagram

Non-radiative decay: The molecule loses its excess energy to the environment without photon emission, usually via vibrational relaxation or interaction with solvent molecules.[1]

Intersystem Crossing (ISC): A non-radiative, spin-forbidden transition from S_1 to the triplet state T_1, enabled by spin–orbit coupling (SOC).[1]

Once in the triplet state (T_1), the molecule has two primary relaxation routes:

Phosphorescence (PH): A radiative but spin-forbidden transition from T_1 to S_0, which occurs more slowly (typically microseconds to seconds) due to the change in spin multiplicity. The presence of heavy atoms can enhance SOC and increase the probability of phosphorescence.[1]

Reverse Intersystem Crossing (rISC): In thermally activated systems, the molecule may undergo **reverse ISC** from T_1 back to S_1, followed by emission via **delayed fluorescence (DF)**. This process has the same spectral characteristics as prompt fluorescence but occurs on longer timescales due to the intermediate triplet state.[1]

The Jablonski diagram is thus a powerful schematic that captures the complex interplay of excitation, relaxation, and emission mechanisms in molecular photophysics. It is widely applicable in fields such as fluorescence spectroscopy, photochemistry, energy transfer studies, and light-harvesting system design.

1.1.2 Franck-Condon Principle

The Franck-Condon Principle is a foundational concept in the study of molecular spectroscopy, providing a framework to understand the relative intensities of vibronic transitions, which involve simultaneous changes in both electronic and vibrational energy levels.[2] This principle, attributed to the early 20th-century work of James Franck and Edward Condon, is rooted in the disparity between electronic and nuclear motion—a notion also central to the Born-Oppenheimer approximation.

When a molecule absorbs or emits light, it undergoes an electronic transition from one energy state to another. These transitions occur on an ultrafast timescale—on the order of femtoseconds (10^{-15} seconds)—which is significantly quicker than the motion of the atomic nuclei. As a result, during the transition, the positions of the nuclei can be considered effectively fixed. The molecule is, therefore, more likely to undergo a vertical transition—a change in electronic state without a simultaneous shift in nuclear coordinates.The probability of such a transition depends on the overlap between the vibrational wavefunctions of the initial and final electronic states. This overlap is described by the Franck-Condon factor, mathematically expressed as the square of the overlap integral between these wavefunctions:

$$F_{if} = |< \Psi_f | \Psi_i i > |^2$$

where Ψ_i and Ψ_f are the vibrational wavefunctions of the initial and final states, respectively. A higher Franck-Condon factor indicates a greater overlap and a stronger transition intensity.

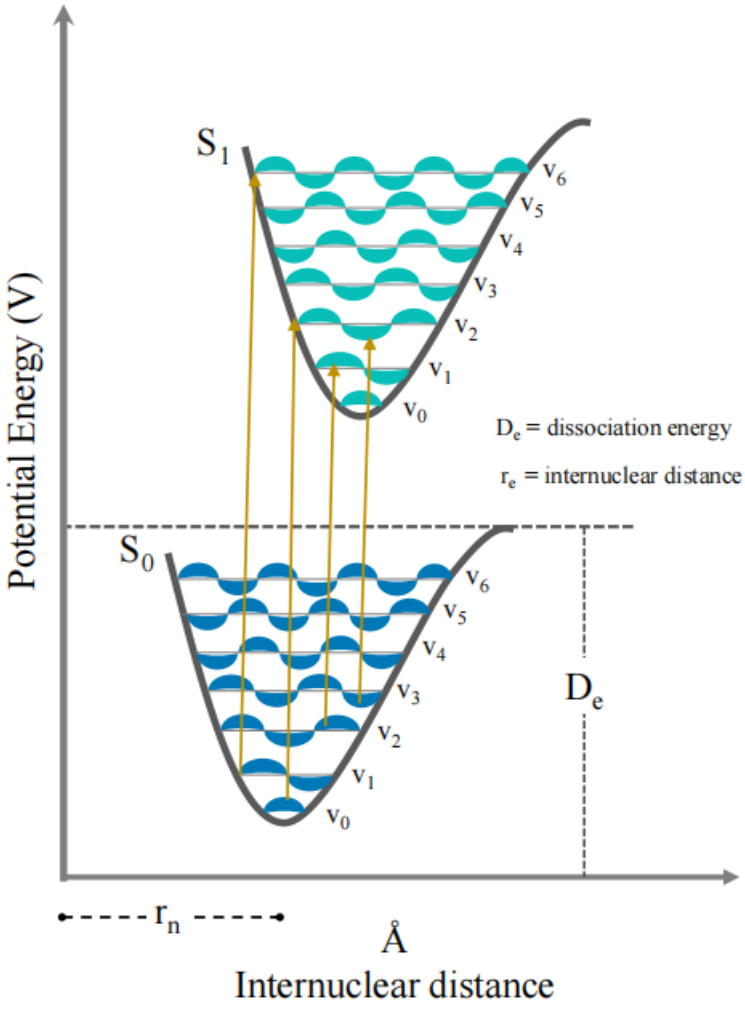

Fig. 1.2: Illustration of the Franck-Condon Principle

Because the equilibrium geometries of the ground and excited states are often different, transitions typically do not occur directly between the lowest vibrational levels of both states. Instead, the electronic transition most often leads to a vibrationally excited level of the new electronic state, resulting in a vibrational progression—a series of peaks—in the absorption or emission spectrum.

The Franck-Condon Principle thus provides key insight into the structure of molecular spectra, explaining why certain vibronic bands are more intense than others and helping to interpret the distribution of spectral features based on molecular geometry changes during excitation or relaxation.

1.1.3 Kasha's rule

Kasha's Rule is a fundamental principle in photophysics, stating that the emission of light—either in the form of fluorescence or phosphorescence—almost always occurs from the lowest excited singlet (S_1) or triplet (T_1) state of a molecule, regardless of the higher excited state (e.g., S_2, S_3) initially populated by light absorption.[3] Once a molecule absorbs a photon and is promoted to a higher electronic excited state, it typically undergoes a series of rapid non-radiative relaxation processes—such as internal conversion and vibrational relaxation—that bring it down to the lowest excited state of the same multiplicity.

These processes occur on extremely fast timescales (typically femto- to picoseconds), well before any radiative emission can take place. As a result, regardless of the excitation wavelength used, the emission spectrum of the molecule remains largely unchanged, as all observable fluorescence or phosphorescence arises from the S_1 or T_1 state, respectively. This behavior ensures that the emission properties are characteristic of the molecule and not dependent on how much excess energy was initially supplied during excitation.

Kasha's Rule thus simplifies the interpretation of photoluminescence spectra and supports the design of fluorescent materials and probes by emphasizing the significance of the lowest excited states in emission processes.

1.2 Radiative Decay Processes

1.2.1 Fluorescence

Fluorescence is a fundamental photophysical phenomenon wherein a molecule absorbs light, typically in the ultraviolet or visible range, and is promoted to an excited singlet electronic state. Following this excitation, the molecule quickly undergoes non-radiative energy loss—such as vibrational relaxation—before it returns to the ground electronic state (S_0) by emitting a photon.[1]

The emission of fluorescence occurs on a very short timescale, typically ranging from picoseconds to nanoseconds. Since some of the absorbed energy is dissipated as heat or through other non-radiative pathways, the emitted photon always has lower energy—and therefore longer wavelength—than the absorbed photon. This energy difference is known as the Stokes shift, and it is a defining characteristic of fluorescent emission.

Fluorescence is highly valued in both research and applied sciences due to its exceptional sensitivity, selectivity, and ability to provide real-time information at the molecular level. It serves as a powerful tool in diverse applications such as fluorescence microscopy, flow cytometry, spectrofluorimetry, and in the design of fluorescent probes and sensors for biological, environmental, and analytical purposes.

1.2.2 Phosphorescence

Phosphorescence is a type of light emission that arises from a molecule transitioning from an excited triplet state (T_1) to the singlet ground state (S_0). This process follows intersystem crossing (ISC), where the molecule undergoes a spin-forbidden transition from an excited singlet state (typically S_1) to a triplet state. Because the $T_1 \rightarrow S_0$ transition involves a change in the electron's spin, it is quantum mechanically forbidden, resulting in a slower rate of emission compared to fluorescence.[1]

The delayed nature of phosphorescence means it can last from microseconds to even seconds, depending on the surrounding environment. Such emissions are often observed under low temperatures, in rigid matrices, or in systems with heavy atoms that enhance spin-orbit coupling, thereby facilitating the otherwise forbidden transition.

Spectrally, phosphorescence is red-shifted relative to fluorescence. This shift occurs because the triplet state is generally lower in energy than the corresponding singlet excited state, meaning the emitted photon has lower energy and a longer wavelength. The efficiency of ISC, and hence phosphorescence, is influenced by the nature of the electronic transitions involved. According to El-Sayed's rule, ISC is more efficient when the transition involves a change in orbital character—for example, from a $\pi \rightarrow \pi^*$ singlet to an $n \rightarrow \pi^*$ triplet state, or vice versa. Transitions within the same orbital type (e.g.,

π→π* to π→π*) are less favorable. Ultimately, the strength of spin-orbit coupling plays a crucial role in determining the rate of ISC and the feasibility of observing phosphorescence. Molecules incorporating atoms with high atomic numbers tend to exhibit stronger phosphorescent behavior due to enhanced coupling between singlet and triplet states.[4]

1.2.3 Delayed Fluorescence

Delayed fluorescence is a luminescent process in which light emission occurs on a longer timescale than prompt fluorescence. It arises from unique relaxation pathways that allow excited molecules to temporarily store energy before releasing it as visible light. Two primary mechanisms are responsible for this phenomenon: E-type (exciton-type)[5] and P-type (photosensitized-type)[6] delayed fluorescence. Both types play critical roles in modern technologies, including organic light-emitting devices (OLEDs), solar energy conversion, and biological imaging.[7–9]

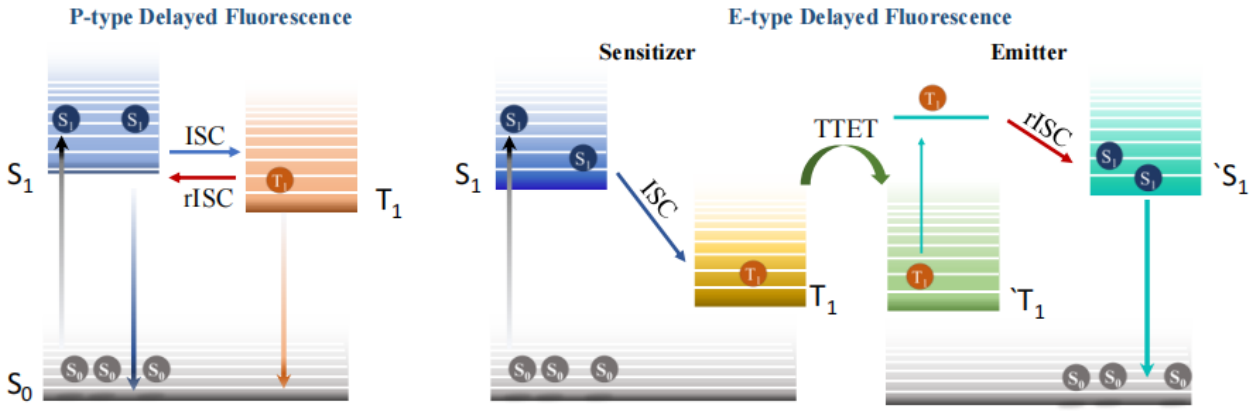

Fig. 1.3: P-type and E-type delayed fluorescence mechanisms.

1.3 Nonradiative Decay Processes

Non-radiative deexcitation refers to transitions between isoenergetic vibrational and rotational levels within electronic states, occurring without the emission of photons. In

electronically excited molecules, the lifetime is largely governed by such non-radiative processes. Within the framework of photophysical behavior, four principal types of non-radiative transitions are typically identified. These processes, often represented by wavy arrows in energy diagrams, play a crucial role in describing how molecules relax from excited states without the release of radiation.[1]

1.3.1 Vibrational Relaxation

Upon absorbing a photon, an electron gains energy that is rapidly redistributed into various vibrational modes of the molecule—a process referred to as vibrational relaxation. This excess energy often manifests as increased kinetic energy within the molecular framework. The fate of this energy—whether it remains localized or is transferred to surrounding molecules—depends significantly on the physical state (solid, liquid, or gas) of the sample. In Jablonski diagrams, vibrational relaxation is typically illustrated with curved arrows between vibrational sublevels of the same electronic state. This ultrafast process occurs on the order of 10^{-14} to 10^{-11} seconds, almost instantaneously following photon absorption. Importantly, since vibrational relaxation is confined to transitions within a single electronic state, it does not involve changes between different electronic energy levels.[1,10]

1.3.2 Internal conversion

Internal conversion is a non-radiative process involving a transition between two electronic states of the same spin multiplicity. This transition is typically followed by vibrational relaxation, allowing the molecule to reach the lowest vibrational level of the excited electronic state. Collisions with surrounding solvent molecules can further influence the redistribution of vibrational energy. On a Jablonski diagram, internal conversion is depicted as a curved arrow connecting vibrational levels of different electronic states. After excitation to a higher electronic state, the molecule may undergo rapid relaxation to the zero-point vibrational level of the first excited state. This process occurs on an ultrafast timescale, typically between 10^{-13} and 10^{-11} seconds.[11]

1.3.3 Intersystem crossing

Non-radiative relaxation between excited states is not restricted to transitions involving states of the same spin multiplicity. When a molecule undergoes relaxation between states of different spin multiplicities, the process is known as *intersystem crossing* (ISC).[11] A common example is the transition from the singlet excited state (S_1) to the triplet state (T_1), as illustrated in Figure 1. Due to the change in spin state, intersystem crossing is generally less probable than internal conversion and thus occurs more slowly, typically on the timescale of approximately 10^{-8} seconds. The efficiency of ISC is significantly enhanced in molecules containing heavy atoms, such as iodine and bromine in organic luminophores, and metal ions in inorganic luminophores, including transition-metal complexes. This enhancement is attributed to stronger spin-orbit coupling—the interaction between an electron's spin and its orbital motion—which increases with heavier atoms. In solution, the presence of paramagnetic species like molecular oxygen can further promote intersystem crossing. Moreover, the likelihood of ISC becomes more pronounced when moving from 3d to 4d and 5d transition metal complexes, owing to the increased spin-orbit coupling in heavier metals.

1.3.4 Reverse Intersystem Crossing

Reverse intersystem crossing (rISC) refers to the transition of a molecule from an excited triplet state back to an excited singlet state, effectively opposing the conventional direction of intersystem crossing (ISC). This process unfolds through several sequential steps. Initially, upon absorbing a photon, the molecule is promoted from its ground state to an excited singlet state. Following this, intersystem crossing may occur, assisted by spin-orbit coupling, allowing the molecule to transition into a triplet excited state of different spin multiplicity. Within the triplet manifold, the molecule can undergo further relaxation processes, such as internal conversion or energy transfer, ultimately populating lower-energy triplet levels. The critical step of rISC then involves the re-promotion of an electron from a triplet state to a singlet state, enabling the molecule to re-enter the singlet excited manifold.[12] Reverse intersystem crossing plays a crucial role in the performance of organic materials, particularly in applications such as organic light-emitting diodes (OLEDs) and organic photovoltaic cells (OPVs), where efficient management of excited state dynamics is essential for enhancing device efficiency and functionality.

1.4 Solvent and Environmental Effect on Absorption Spectra

The photophysical properties of organic chromophores and fluorophores, such as their absorption and emission behavior, are profoundly influenced by their surrounding environment. Among the most critical environmental factors is the solvent medium, which can significantly affect the position, intensity, and shape of electronic spectra. This phenomenon, often referred to as **solvatochromism**, arises from the interaction between the electronic states of the molecule and the polarity or polarizability of the solvent.[1,13,14]

In absorption spectroscopy, solvent polarity can lead to shifts in the electronic transition energies, typically manifesting as bathochromic (red) or hypsochromic (blue) shifts in the absorption maxima. These shifts depend on the relative stabilization of the ground and excited states of the molecule in different solvent environments.

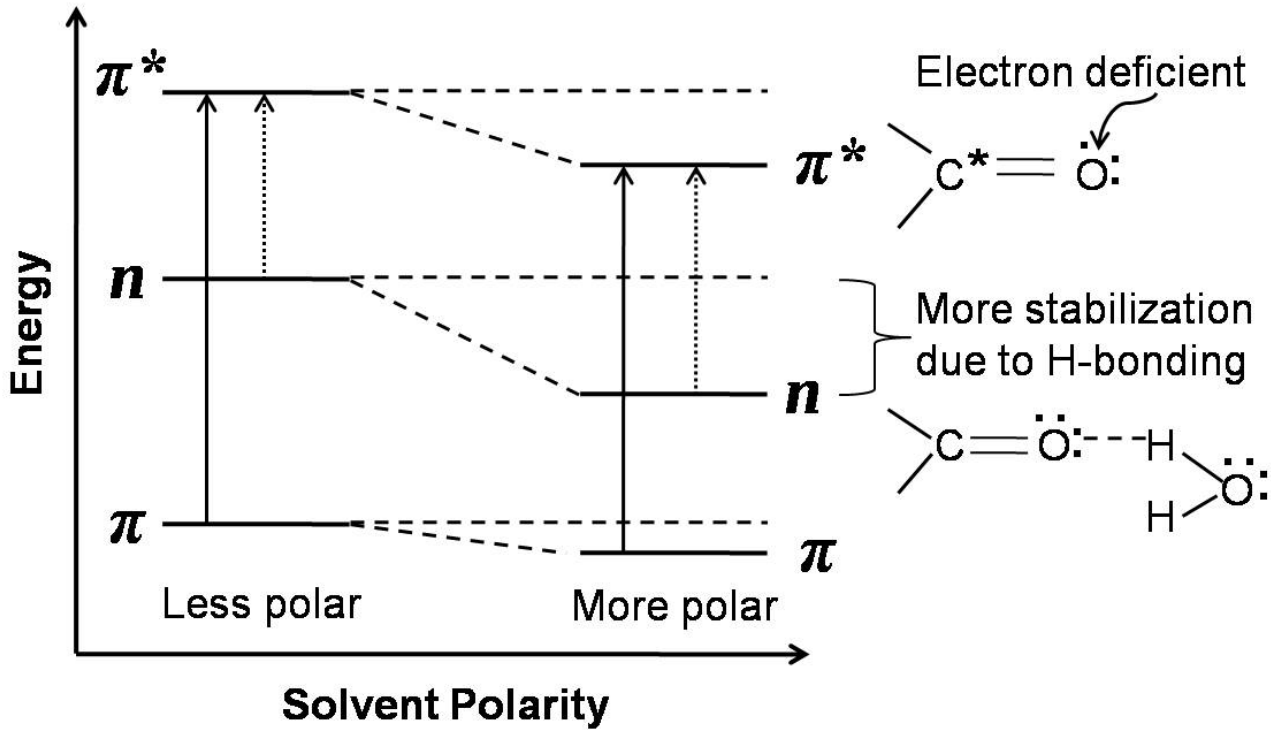

Fig. 1.4: Effect of solvent polarity on n→π* and π →π* transitions.

π^*-orbital is more polar than π therefore in polar solvents it will stabilize more and π to π^* transition undergoes bathochromic shift or red shift with increasing polarity of solvents.

Non-bonding n -orbital is more polar than π^*-orbital therefore in polar solvents it will stabilize more and n to π^* transition undergoes hypsochromicc shift or blue shift with increasing polarity of solvents.

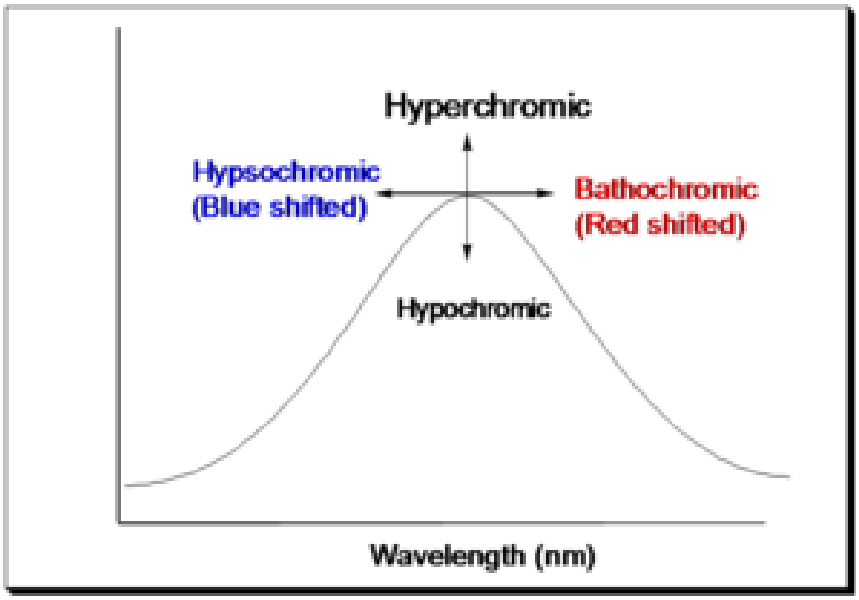

Fig. 1.5: Bathochromic, Hypsochromic, Hyperchromic, Hypochromic shifts summarized.

1.5 Solvent and Environmental Effect on Emission Spectra

The fluorescence emission characteristics of fluorophores are highly sensitive to the polarity of the solvent and the nature of the surrounding environment. These environmental effects are not solely governed by solvent polarity but arise from a combination of interrelated factors that influence the excited-state behavior of the molecule. Collectively, these factors can alter both the spectral profile and fluorescence quantum yield.

Key influences on fluorescence emission and efficiency include:

1. Solvent polarity and viscosity [15]

2. Solvent relaxation dynamics [16]

3. Conformational flexibility of the fluorophore [17]

4. Rigidity of the microenvironment [18]

5. Intramolecular charge transfer (ICT) [19]

6. Excited-state proton transfer and other photochemical processes [20,21]

7. Intermolecular interactions between fluorophores [22]

8. Modulation of radiative and non-radiative decay rates [23]

1.5.1 Effects of solvent polarity

Fluorophores typically emit light at longer wavelengths than those at which they absorb, a phenomenon known as the Stokes shift. This red-shifted emission results from various relaxation processes that occur after a molecule absorbs light. Upon excitation, the fluorophore generally transitions to a higher vibrational level of the first excited singlet state (S_1). The excess vibrational energy is rapidly dissipated to the surrounding solvent, leading to vibrational relaxation. If the molecule is excited to a higher electronic state such as S_2, it undergoes rapid internal conversion to S_1 on the order of 10^{-12} seconds.

Solvent molecules play a crucial role in modulating the photophysical behavior of fluorophores, especially emission properties. In polar solvents, the excited state—often possessing a greater dipole moment than the ground state—is stabilized due to solvent reorientation around the excited-state dipole. This stabilization lowers the energy of the excited state, resulting in a red shift (longer wavelength) of the emission maximum. As solvent polarity increases, this effect becomes more pronounced. Polar fluorophores, in particular, exhibit significant solvent-dependent emission shifts, whereas nonpolar

molecules like simple aromatic hydrocarbons show minimal sensitivity to solvent polarity.

Fluorescence lifetimes, typically in the nanosecond range (1–10 ns), are much longer than the timescale of solvent relaxation, which occurs within 10–100 picoseconds in fluid solvents at room temperature. As a result, fluorescence emission reflects the fully relaxed state of the solvent-fluorophore system. In contrast, absorption events occur extremely rapidly (10^{-15} seconds), far faster than solvent or molecular reorientation can occur. Thus, absorption spectra are less influenced by solvent polarity because both the ground and excited states experience the same unrelaxed environment at the moment of photon absorption. Emission, however, arises from a state where the solvent has reoriented around the excited-state dipole, making it far more responsive to changes in solvent properties.

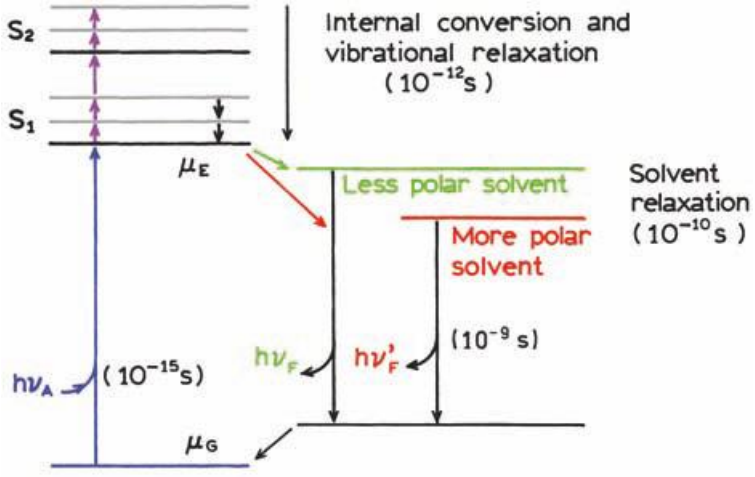

Fig. 1.6 : Jablonski diagram for fluorescence with solvent relaxation.

1.6 Fluorescence Quenching

Fluorescence quenching encompasses any process that leads to a reduction in the fluorescence intensity of a system.[24,25] This phenomenon can arise from a variety of molecular interactions, including excited-state chemical reactions, conformational changes, energy transfer mechanisms, ground-state complex formation, and collisions

between fluorophores and quenching agents. In this study, the primary focus is on dynamic or collisional quenching, which occurs due to direct encounters between the excited fluorophore and the quencher molecule. Static quenching, which results from the formation of non-fluorescent complexes in the ground state, is also considered, as it can provide important insights into binding interactions between the fluorophore and the quencher. However, static quenching may complicate data interpretation if not properly accounted for. Additionally, decreases in fluorescence intensity may sometimes be attributed to optical artifacts, such as high absorbance or sample turbidity. These non-molecular effects, often referred to asapparent or trivial quenching, do not reflect underlying molecular processes and are excluded from consideration in the present analysis.

1.6.1 Collisional Quenching

Collisional quenching, also referred to as dynamic quenching, occurs when an excited fluorophore encounters a quencher molecule through random molecular collisions, resulting in non-radiative deactivation of the excited state.[26] This process is quantitatively described by the Stern–Volmer equation, which relates the fluorescence intensities in the absence (F_0) and presence (F) of the quencher to the quencher concentration ([Q]). The Stern–Volmer relationship is expressed as

$$\frac{F_0}{F} = 1 + K_{sv}[Q] = 1 + K_q\tau_0[Q]$$

where k_q is the bimolecular quenching rate constant and τ_0 is the unquenched fluorescence lifetime.[27] Alternatively, the product $k_q\tau_0$ is represented by the Stern–Volmer constant (K_{sv}). In systems dominated by dynamic quenching, a plot of F_0 / F against [Q] yields a linear relationship, with the slope corresponding to K_{sv}. A linear Stern–Volmer plot indicates that the fluorophores are uniformly accessible to the quencher, while deviations from linearity may suggest the presence of multiple populations of fluorophores with differing accessibility. The magnitude of K_{sv} provides insights into the quenching efficiency: higher values imply more effective quenching, potentially approaching diffusion-controlled limits.

1.6.2 Static Quenching

In the preceding section, quenching arising from diffusive collisions between the excited-state fluorophore and quencher was discussed. This type of quenching is inherently time-dependent, occurring during the lifetime of the excited state. Alternatively, quenching can also occur through the formation of a non-fluorescent ground-state complex between the fluorophore and quencher. Upon light absorption, this complex promptly returns to the ground state without emitting a photon.

In the case of static quenching, the relationship between fluorescence intensity and quencher concentration can be described using the association constant (K_S) for complex formation.[28,29] This constant is defined as:

$$K_s = \frac{[F - Q]}{[F][Q]}$$

where [F-Q] is the concentration of the non-fluorescent complex, [F] is the concentration of free fluorophore, and [Q] is the concentration of quencher. Assuming that the complex is completely non-fluorescent, the remaining fluorescence (F/F_0) corresponds to the fraction of non-complexed fluorophores. Given that the total fluorophore concentration $[F]_0$ equals the sum of free and complexed species, substitution into the association constant expression leads to a linear dependence of F_0 / F on [Q].

This linearity mirrors that observed in dynamic quenching, making it difficult to distinguish between static and dynamic mechanisms based solely on fluorescence intensity measurements. However, additional methods, such as fluorescence lifetime analysis, can differentiate between the two. In static quenching, the non-fluorescent complex removes a fraction of the fluorophores without altering the excited-state lifetime of the uncomplexed fluorophores, thus $\tau_0/\tau = 1$. In contrast, dynamic quenching results in a proportional decrease in both fluorescence intensity and lifetime, where $F_0/F = \tau_0/\tau$.

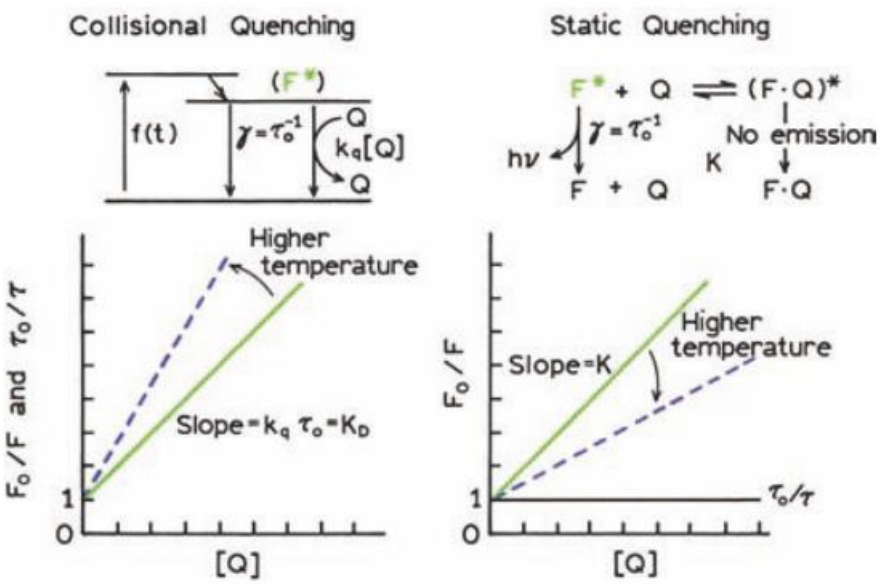

Fig. 1.7 : Comparison of dynamic and static quenching.

Absorption spectroscopy also serves as a useful tool for distinction. Since dynamic quenching impacts only the excited state, it does not alter the absorption spectrum of the fluorophore. However, ground-state complex formation often induces noticeable changes in the absorption profile. Therefore, careful examination of spectral changes, alongside lifetime measurements, provides a comprehensive approach to accurately distinguishing between static and dynamic quenching mechanisms.

1.7 Introduction

Oxazoles are a class of five-membered heterocyclic aromatic compounds containing one oxygen and one nitrogen atom at the 1 and 3 positions, respectively. These heterocycles are of significant interest in both synthetic and medicinal chemistry due to their unique electronic properties and broad biological activities. Naturally occurring and synthetic oxazole derivatives have demonstrated antibacterial, antifungal, anti-inflammatory, anticancer, and antiviral properties, making them valuable scaffolds in drug design. In addition to their pharmaceutical applications, oxazoles are also utilized in materials science, particularly in the development of fluorescent dyes and organic electronic devices, owing to their tunable photophysical characteristics. Their versatility and ease of

functionalization have led to the widespread use of oxazoles in various chemical, biological, and industrial applications.[30,31]

Oxazole-based compounds, owing to their rigid aromatic structure and extended π-conjugation, have gained prominence in biophysical and biomedical research. The cyclization of Schiff bases into oxazole derivatives not only improves the fluorescence efficiency and stability of these compounds but also significantly influences their interaction profile with biological macromolecules such as proteins.[32,42]

Among these, Bovine Serum Albumin (BSA) serves as a prototypical model for exploring protein-ligand interactions due to its structural homology with Human Serum Albumin (HSA) and its well-characterized binding domains.[43,44]

Bovine serum albumin (BSA) is a globular protein derived from the blood plasma of cattle and is widely used as a model protein in biochemical and biophysical research. Comprising approximately 583 amino acid residues, BSA has a molecular weight of around 66 kDa and is structurally organized into three homologous domains (I, II, and III), each containing two subdomains (A and B). Its predominantly α-helical structure and high solubility make it an ideal subject for studying protein–ligand interactions, protein folding, and conformational changes.[45]

Biologically, BSA plays a critical role in maintaining osmotic pressure and transporting a wide range of endogenous and exogenous substances, including fatty acids, hormones, and various drugs. Due to its structural and functional similarity to human serum albumin (HSA), BSA is frequently used as a surrogate in pharmacological studies to investigate drug binding, protein dynamics, and molecular recognition processes. Its stability, non-immunogenic nature, and availability further contribute to its extensive use in diagnostics, drug delivery systems, and biotechnological applications. Understanding how small molecules interact with BSA provides valuable insights into their potential bioavailability, distribution, and therapeutic efficacy in vivo.[46]

The interaction of oxazole derivatives with BSA is primarily governed by non-covalent forces such as hydrogen bonding, π-π stacking, electrostatic interactions, and hydrophobic effects. These interactions can induce conformational changes in the protein,

which are often monitored using spectroscopic techniques such as UV-Vis, fluorescence emission, and circular dichroism (CD).

In particular, fluorescence quenching studies provide valuable insights into the binding mechanism—distinguishing between static and dynamic quenching—and allow for the calculation of key thermodynamic parameters such as the binding constant (K_a), number of binding sites (n), enthalpy (ΔH), and entropy (ΔS). These parameters reveal not only the strength and spontaneity of the interaction but also the nature of the binding forces, offering deeper understanding of the biocompatibility and in vivo behavior of the oxazole derivative.

1.8 Aim and objective of the thesis

The aim of this thesis is to design and synthesize a novel oxazole derivative with enhanced photophysical and biophysical properties, with the goal of exploring its potential applications in fluorescence-based sensing, bioimaging, and protein-binding studies. By introducing strategic functional groups, the study seeks to improve the compound's optical characteristics, stability, and interaction capabilities, thereby contributing to the development of advanced molecular probes for spectroscopic and biomedical applications.

1.9 Objectives of the work

1. To design a novel oxazole derivative.

2. Synthesis and characterization of the designed molecule

3. Complete spectroscopic analysis of novel oxazole derivative through uv-vis spectrophotometer, steady state fluorescence measurement, and time resolved fluorescence measurement through Time correlated Single Photon Counting setup.

4. Spectroscopical analysis novel oxazole derivative and to explore the potential biological relevance of the cyclized system, with bovine serum albumin (BSA), a model transport protein.

CHAPTER – 2
MATERIALS AND METHODS

This chapter deals with the materials, methodologies for synthesis of RSM which is synthesized by our group, sample preparation, and techniques employed for a thorough spectroscopic investigation. It discusses various characterization techniques, such as UV-visible absorption spectroscopy conducted with a spectrophotometer, steady-state fluorescence, and fluorescence lifetime measurements via time-correlated single photon counting (TCSPC). The intricacies of the instrumentation and the strategies for data acquisition are comprehensively reviewed. Additionally, the chapter delves into quantum chemical calculations, which include the optimization of ground state (GS) and excited state (ES) structures as well as orbital analysis. These computational evaluations are performed using density functional theory (DFT) and time-dependent density functional theory (TD-DFT) utilizing the Gaussian software package. For the investigation of RSM-BSA binding interaction molecular docking study is carried out.

2.1 Materials

4-(Diethylamino)salicylaldehyde, 4-amino-3-hydroxy-1-naphthalenesulfonic acid ethanol, were procured from Sigma Aldrich (India) and utilized without further modification. The spectroscopic-grade solvents, namely n-heptane, hexane, toluene, 1,4-dioxane, tetrahydrofuran (THF), chloroform ($CHCl_3$), dichloromethane (DCM), dimethylformamide (DMF), acetonitrile (ACN), butanol, isopropanol, ethanol, and methanol (MeOH), were acquired from Fischer Scientific, India, and employed as received. BSA and HEPES buffer is procured from SRL, India and used as it is. Ibuprofen and Warfarin are purchased from Bangalore Fine chemicals, India. Stock solutions of BSA, and is prepared in 50 mM HEPES buffer (pH = 7.4) and stored at 4°C.

Concentrated stock solution of RSM (1 mM), ibuprofen (3 mM), and warfarin (3mM) are prepared in spectroscopic grade 1, 4- dioxane. Distilled water is used wherever required.

2.2 Synthesis of RSM

1-Amino-2-hydroxy-4-naphthalenesulfonic acid (1 mM) was dissolved in 20 mL of ethanol, followed by the addition of sodium hydroxide (1 mM).

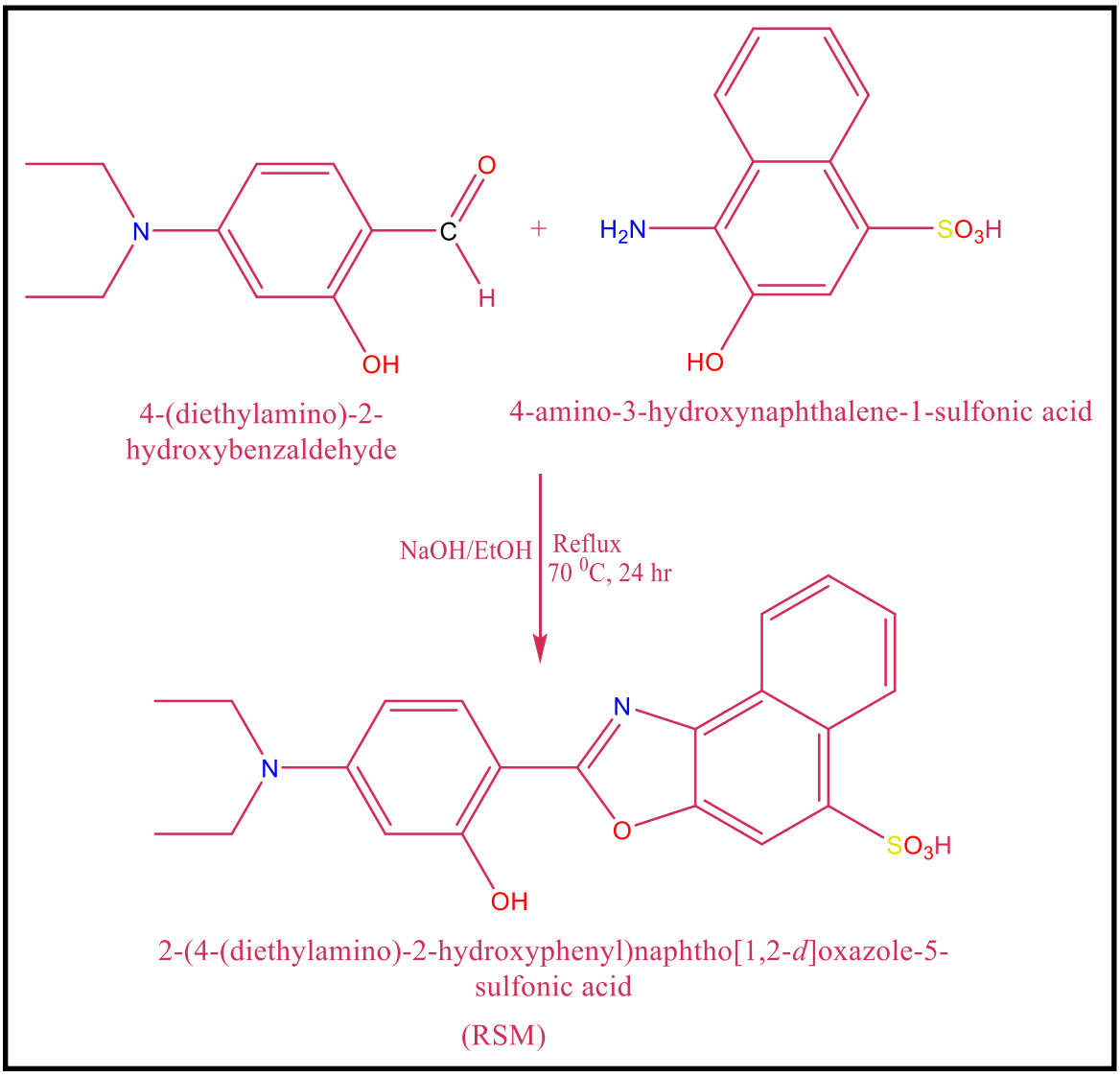

Fig. 2.1 : Synthetic route of RSM.

The reaction mixture was stirred for approximately 10 minutes at room temperature until a clear solution was formed. To this solution, 4-(diethylamino)salicylaldehyde (1 mM) was added, and the mixture was heated at 70 °C under continuous stirring for 24 hours to facilitate the reaction. Upon completion of the reaction, the mixture was cooled to room temperature and neutralized with dilute hydrochloric acid. The resulting mixture was then subjected to a liquid-liquid extraction using ethyl acetate and water to separate the organic components. The organic phase was collected, dried over anhydrous sodium sulfate, and concentrated under reduced pressure. The crude product was subsequently purified by column chromatography using a mixture of ethyl acetate and petroleum ether as the eluent to afford the desired product in pure form.

2.3 Instrumentation and methodology

2.3.1 UV-vis Spectrophotometer

Measuring the transmittance or absorbance of a sample in response to electromagnetic radiation is accomplished through the employment of a UV-vis spectrophotometer. Typically covering a comprehensive spectrum of electromagnetic wavelengths, these instruments evaluate the optical properties of samples within the ultraviolet and visible ranges, generally spanning from 190 to 900/1100 nm. UV-vis spectrometers discern the contrast between the incident radiation (I0) and the transmitted radiation (It) as light traverses or is reflected by a material. The photons absorbed by UV-vis light possess sufficient energy to facilitate transitions between electronic states.

The wavelength of light that is absorbed signifies the energy necessary for an electron to transition from a lower to a higher energy state. Typically, the presence of an absorbance band at a specific wavelength suggests the existence of a chromophore. A spectrum of physicochemical characteristics of substances can be revealed through UV-visible spectroscopy, which offers vital information for their identification. The impact of path length (b), measured in centimeters, on transmittance (S) was initially articulated by Bouger in 1729; however, it is Lambert (1760) who is chiefly recognized for providing the foundational mathematical representation of this relationship. The mathematical formulation can be expressed as:

$$T = \frac{I_t}{I_0} = e^{-kb}$$

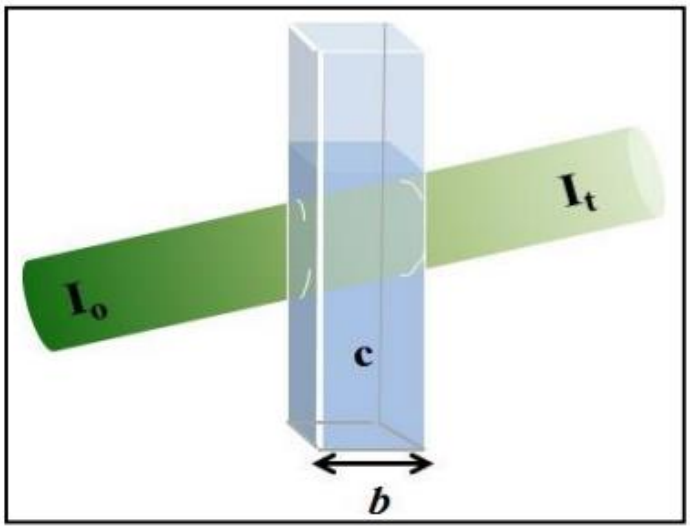

Figure 2.2 : The Beer-Lambert Law.

In this equation, k indicates a constant, while *e* denotes the base of natural logarithms. Beer's law is fundamentally parallel to Bouguer's law, with the primary differentiation being its expression in terms of concentration (c), quantified in moles per liter. The degree of light absorption is directly proportional to the count of absorbing molecules that the light interacts with. The Beer-Bouguer-Lambert law is derived from the synthesis of these two principles.

$$T = \frac{I}{I_0} = e^{-kbc}$$

This equation can be articulated in a linear form through the application of logarithmic transformation and is conventionally represented in decadic form:

$$A = -\log T = -\log\frac{I_t}{I_0} = \log\frac{I_0}{I_t} = \varepsilon bc$$

In this context, ε represents the molar extinction coefficient, expressed in $Lg^{-1}cm^{-1}$. The principle widely termed as Beer's law or Beer-Lambert law claims that the absorbance of light is directly proportional to the product of the medium's thickness through which the light is transmitted and the concentration of the absorbing chromophore.[46] (Figure 2.2)

A spectrophotometer is comprised of several essential components: (i) a source that produces a comprehensive spectrum of electromagnetic radiation, (ii) a mechanism that differentiates and selects a particular wavelength of light, (iii) a designated area for sample placement, and (iv) one or more detectors for evaluating the intensity of the radiation. Additional optical elements, such as lenses or mirrors, assist in directing light through the apparatus. Numerous types of spectrophotometers can be acquired, including single-beam, double-beam, and split-beam formats. Each model presents distinct advantages and limitations. In a standard single-beam spectrophotometer, the blank and the sample are measured sequentially, with an elapsed time of several seconds for a single wavelength measurement and potentially several minutes for a complete spectral assessment. Lengthy time intervals may result in considerable inaccuracies in bulb intensity. Alternatively, a double-beam spectrophotometer is specifically designed to account for fluctuations in lamp intensity that may arise during the measurement of blank and sample cuvettes.

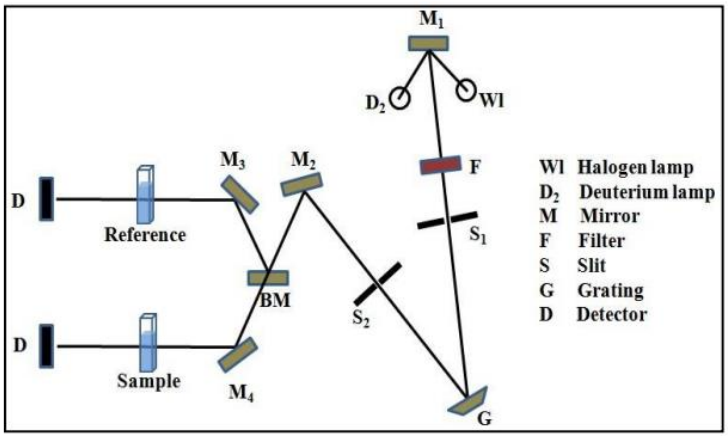

Figure 2.3 : Optical system diagram of double-beam UV-vis spectrophotometer JASCO V-630.

The UV-Vis absorption spectra were acquired at a temperature of 298 K using a double-beam Jasco V-630 spectrophotometer, which includes a 1.0 cm quartz cell. Figure 2.3 showcases the dual light sources employed in the UV-Visible spectrophotometer. Ultraviolet light is emitted by a deuterium (D2) lamp, functioning within the wavelength range of 190 to 350 nm. In contrast, visible light is generated by a halogen (Wl) lamp, which emits light across the spectrum of 330 to 1100 nm. Following its reflection from mirror 1, the light beam passes through a narrow aperture before encountering a diffraction grating. The grating housed within the monochromator disperses the light through scattering, subsequently focusing it onto the exit slit.

The light that exits through the slit is meticulously filtered to allow only a sole wavelength, thus ensuring it remains monochromatic. A precise filter is utilized to eliminate any unwanted higher-order diffraction. The light beam is subsequently directed toward a beam splitter, which delineates the beam into two distinct trajectories. One trajectory is aimed at the sample designated for measurement, while the other is channeled toward the reference sample. Thereafter, the detector evaluates the intensities of the light beam at its terminus.

2.3.2 Spectrofluorometer

Fluorescence spectroscopy and fluorescent probes are fundamental techniques utilized across a broad spectrum of fields in contemporary medicine and research, including molecular biology, biophysics, biochemistry, clinical diagnostics, as well as analytical and environmental chemistry. These approaches are highly esteemed for their remarkable sensitivity, exceptional spatial resolution, rapid responsiveness, and considerable versatility. Fluorescence describes the phenomenon by which a fluorophore emits light when it transitions from an electronically excited singlet state. When the fluorophore is excited by a spectrofluorometer, it captures photons at a particular wavelength and subsequently emits photons at a different wavelength. Spectrofluorometers are specifically crafted to measure the fluorescence characteristics of a fluorophore by identifying its discrete excitation and emission wavelengths. The fluorescence signature obtained can be linked to the concentration and the chemical context of the fluorophore.

The Jasco FP-8300 spectrofluorometer is utilized to acquire the steady-state emission, excitation, synchronous, and three-dimensional fluorescence spectra. A 1.0 cm quartz

cell, together with an external slit width of 2.5 nm, is employed for this examination. The fluorescence spectra pertinent to the tubulin-CBIQD interactions are measured using a 1.0 cm path length 9FL Semi-Micro fluorescence cuvette. Figure 2.4 depicts the schematic architecture of a spectrofluorometer. This instrument employs a xenon (Xe) lamp as its light source for illumination. These lamps are particularly advantageous due to their significant intensity across the entire wavelength range, commencing from 250 nm. The light emitted by the Xe lamp is meticulously directed towards the entry slit S1 of the excitation monochromator, facilitated by the ellipsoidal mirror M1 and the spherical mirror M0.

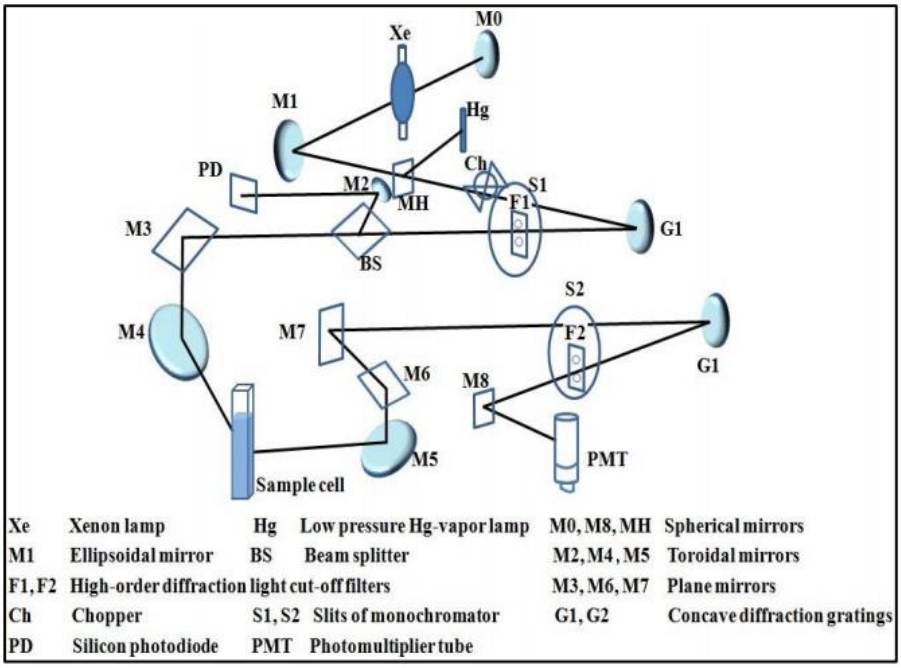

Figure 2.4 : Optical system diagram of spectrofluorometer FP-8300

The light that passes through the slit is dispersed by the diffraction grating G1, permitting only light of a particular wavelength to proceed through the exit slit. The excitation monochromator is equipped with a pair of gratings that efficiently minimize the occurrence of stray light, which corresponds to wavelengths that differ from the selected frequency. These monochromators employ concave gratings, meticulously designed through advanced holographic techniques, to further curtail the incidence of

unwanted light. A segment of the monochromatic light is diverted towards the monitoring detector (silicon photodiode) PD through the beam splitter BS. The remaining monochromatic light that advances through the BS is directed to the sample compartment utilizing the plane mirror (M3) and the toroidal mirror (M4), where it is focused at the intersection of the sample cell. The emission generated from the sample cell is directed towards the entrance of slit S2 in the emission monochromator with the aid of the toroidal mirror (M5) and plane mirrors M6 and M7. The light emitted from exit slit S2 is then conveyed to the electromagnetic (EM) detector PMT, which can be considered a current source.

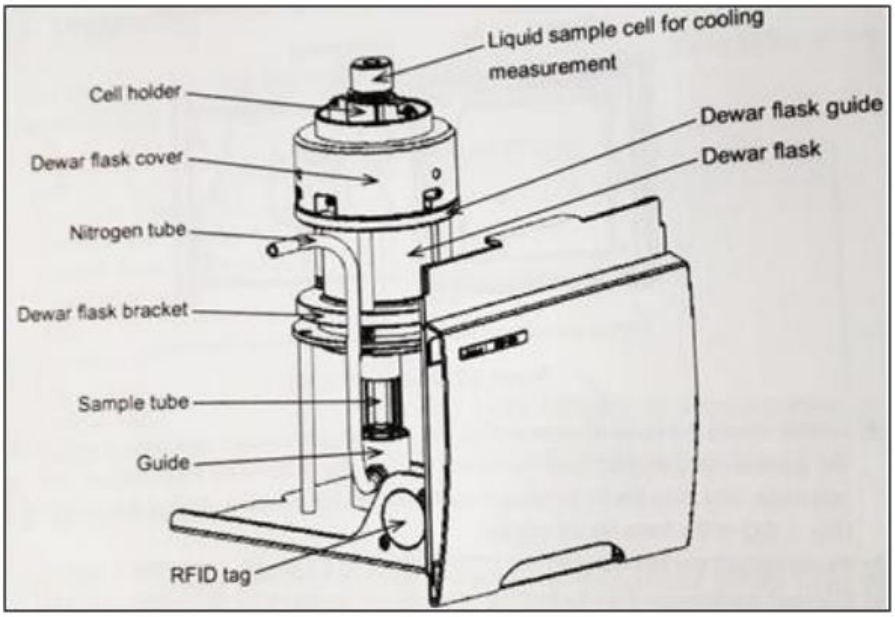

Figure 2.5 : Liquid Nitrogen Cooling unit of PMU-830 phosphorescence accessory of spectrofluorometer FP-8300 used for phosphorescence measurements.

In this context, the current elicited by the photomultiplier tube (PMT) is directly linked to the intensity of the incident light. Photomultiplier tubes are distinguished by their capability to detect and respond to individual photons. The resultant pulses may be interpreted as an average signal or enumerated as distinct photon occurrences. This spectrofluorometer enables the precise documentation of both excitation and emissionspectra. An emission spectrum typifies the spectrum of wavelengths emitted by a substance when it is excited at a particular wavelength. Conversely, the excitation

spectrum illustrates the variations in fluorescence intensity as the excitation wavelength alters while the observed emission wavelength remains constant.

The instrument's sample chamber is furnished with shutters, a magnetic stirrer, and two filter holders. These holders are strategically positioned on both the excitation and emission sides and can accommodate either an attenuator or polarizers as required. Shutters are implemented to obstruct incoming light or to block the transmission of light. Polarizers are utilized in both the excitation and emission light channels specifically for the measurement of fluorescence anisotropy or when it is necessary to isolate particular polarized components of the emission and/or excitation. The FP-8300 spectrofluorometer is equipped with a removable cell holder, making it easy to attach the PMU-830 phosphorescence accessory for conducting phosphorescence measurements. The nitrogen (N2) purge connection serves to ensure a continuous supply of N2 gas, maintain anaerobic conditions during phosphorescence measurements, and, most importantly, prevent condensation around the sample measurement point of the Dewar flask.

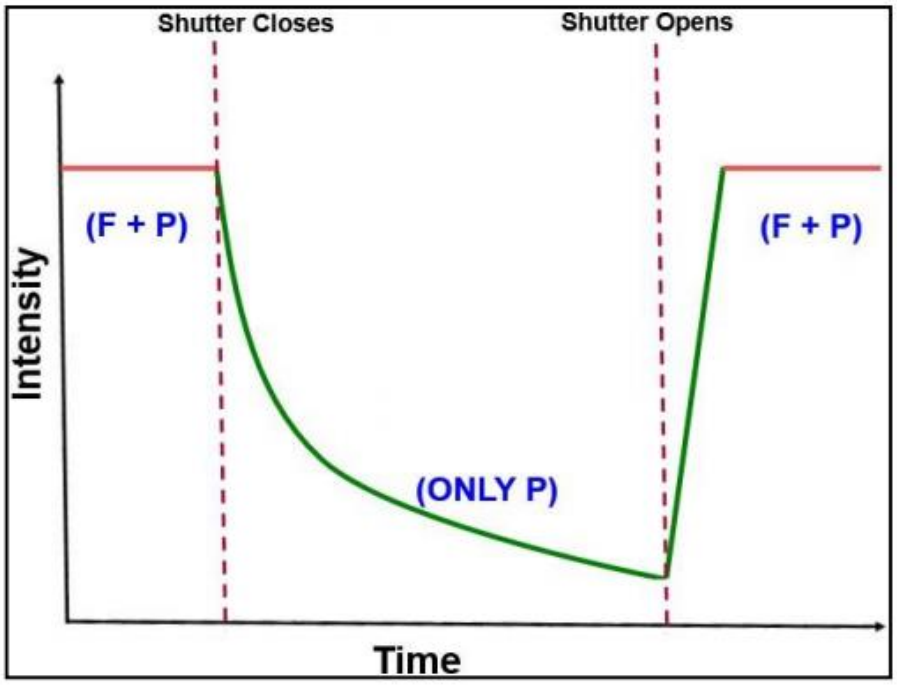

Figure 2.6 : Condition of shutter and observed signal; F and P represent fluorescence and phosphorescence respectively.

The PMU-830 liquid nitrogen sampling accessory, which contains the quartz capillary tube (LPH-140 liquid sample cell) for holding the sample (illustrated in Figure 2.5), can be effortlessly exchanged for the standard cell compartment. It serves to obtain phosphorescence spectra.

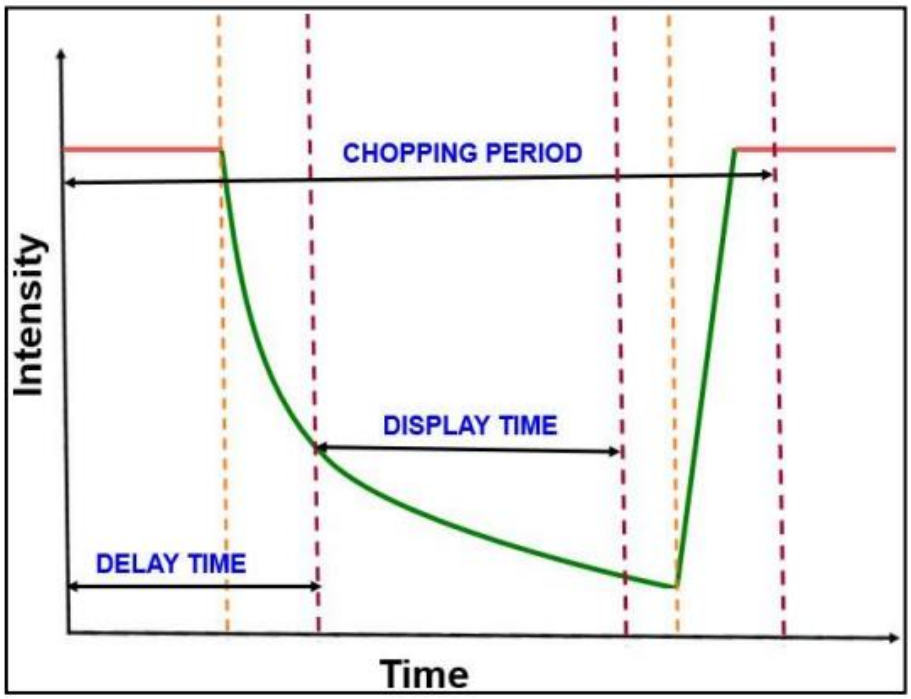

Figure 2.7 : Relation between [Delay Time], [Display Time] and [ChoppingPeriod] on phosphorescence lifetime measurement.

The FP-8300 spectrofluorometer is equipped to detect phosphorescence while allowing for meticulous evaluations of phosphorescence lifetimes. This capability is facilitated by a continuously rotating shutter within the excitation monochromator. Figure 2.6 illustrates the scenario wherein the shutter perpetually alternates between the "Open" and "Close" settings. It also presents the emitted signals corresponding to both fluorescence and phosphorescence from the sample. When the shutter opens, the sample is subjected to excitation light, resulting in a combined signal that encompasses both fluorescence and phosphorescence. Conversely, when the shutter is closed, only the phosphorescent emission is detected.To obtain a phosphorescence signal without fluorescence interference, it is critical to set the appropriate delay time and display time for phosphorescence lifetime measurements, as shown in Figure 2.7. The "Delay Time" refers to the interval between the start of the measurement and the moment when the

interfering fluorescence is no longer detectable. "Display Time" represents the duration for which the time-course data is shown on the measurement screen.Additionally, the "Chopping Period" is the cycle during which the camera shutter alternates between open, closed, and open again. By adjusting the chopping period, the software can be calibrated to suit samples with a wide range of lifetimes, from short to long.

2.3.3 Time-resolved fluorescence spectroscopy

Understanding the dynamics of excited states is fundamental to elucidating photophysical, photochemical, and photobiological processes. Time-resolved fluorescence spectroscopy is a powerful tool for probing these dynamics, with three widely employed techniques for measuring fluorescence lifetimes: the stroboscopic (strobe) method, pulse fluorometry or time-correlated single photon counting (TCSPC), and phase-modulation fluorometry. The strobe and TCSPC techniques are time-domain methods, whereas phase-modulation fluorometry operates in the frequency domain.

Pulse fluorometry involves the use of a short excitation pulse to generate a δ-pulse (Dirac-pulse) response from the sample, which is subsequently convolved with the instrument response function. Phase-modulation fluorometry, on the other hand, utilizes sinusoidally modulated excitation light across a range of frequencies to obtain the sample's harmonic response, which corresponds to the Fourier transform of the δ-pulse response.

The time-domain techniques—strobe and TCSPC—are similar in terms of the parameters measured and the analytical approaches employed. The key differences between them lie in the hardware configuration, particularly in the design of the pulsed light sources and detection electronics. Nonetheless, certain light sources can be adapted for use in both methods.

The measurements were performed using a PTI Time-Resolved Spectrofluorometer PicoMaster (HORIBA, USA), employing 540 nm and 280 nm LEDs as excitation sources. These LEDs typically produce pulse widths between 700 and 1100 picoseconds, depending on the specific diode used. Detection was carried out using a PMD-2 detector,

which has a response time of approximately 180 picoseconds and a temporal resolution of around 813 femtoseconds. The detector is designed for uniform response across the photocathode and supports a broad emission detection range from 185 to 820 nm.

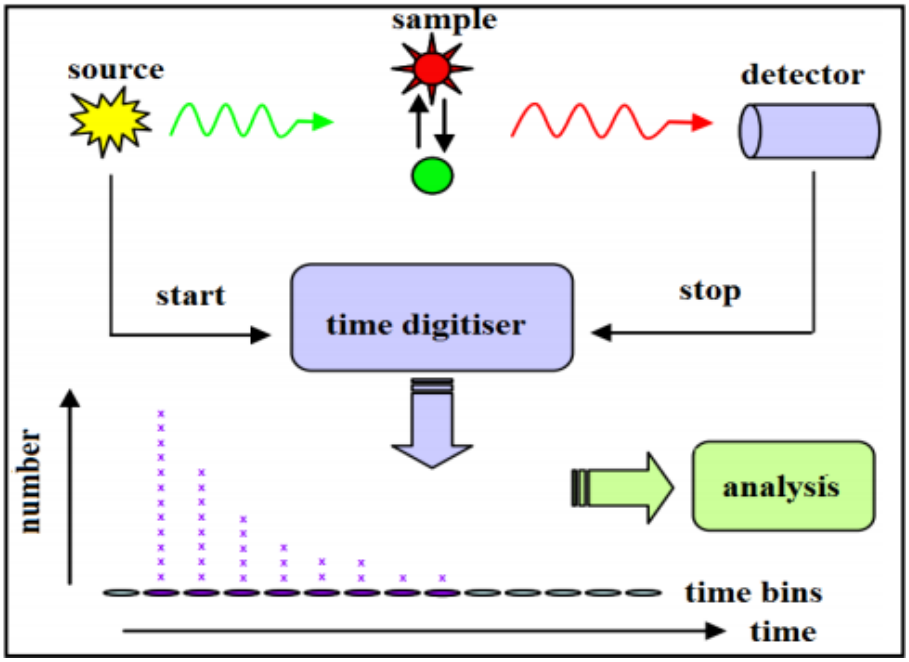

Figure 2.8 : Schematic representation of TCSPC

Data were analyzed using FelixGX 4.1.2 software, which is specialized for decay fitting and fluorescence lifetime analysis. The quality of the exponential fits was validated using the reduced chi-squared (χ^2) statistic and by examining the randomness of the residuals. For systems exhibiting biexponential decay, the average fluorescence lifetime $\langle \tau \rangle$ was calculated using the decay times (τ_i) and the corresponding pre-exponential factors (α_i) according to the following relation:

$$\langle \tau \rangle = \frac{\sum \tau_i \alpha_i}{\sum \alpha_i}$$

Time-Correlated Single Photon Counting (TCSPC) is a precise and widely used technique for measuring fluorescence lifetimes by detecting the arrival times of individual photons emitted from a sample following pulsed excitation. In this method, a

pulsed light source—typically a laser or LED—is used to excite the sample, as illustrated in Figure 2.8. Each excitation pulse triggers the timing electronics, marking the "start" of the measurement cycle. When a fluorescence photon is subsequently detected, it generates a "stop" signal, and the time interval between the excitation and detection is recorded.

These time intervals are sorted into a histogram consisting of discrete time bins of width Δt. Each photon detected within the interval t to $t + \Delta t$ is assigned to the corresponding time bin. Repeating this process over many cycles allows for the construction of a time-resolved fluorescence decay profile.

The width of the time bins directly affects the temporal resolution of the system—narrower bins provide higher resolution but may require longer acquisition times to gather sufficient data for accurate lifetime determination.

The TCSPC system employs advanced electronic components to accurately measure the time delay between the detection of individual fluorescence photons and corresponding reference pulses generated by a lamp control unit or a secondary detector (as depicted in Figure 2.9). Upon excitation, the LED emits a light pulse that simultaneously excites the sample and sends a timing signal to the electronics.

Both the reference pulse and the detected single-photon signal are processed through Constant Fraction Discriminators (CFDs). CFDs are designed to improve timing precision by filtering out low-amplitude noise and generating a trigger signal when a defined fraction of the pulse height is reached. This method ensures that the timing is independent of the amplitude of the incoming pulse, thereby minimizing timing jitter and enhancing the temporal resolution of the TCSPC measurement.

To reduce timing jitter that can result from triggering on fixed pulse amplitudes, the TCSPC system employs a Constant Fraction Discriminator (CFD), which ensures precise timing by generating a trigger at a consistent fraction of the pulse height. This approach allows for more accurate determination of photon arrival times.

The Time-to-Amplitude Converter (TAC) is activated by the detection of a single photon, initiating a voltage ramp that decreases linearly over time. This ramp continues until it is

stopped by a corresponding reference pulse. A reference pulse is generated for each excitation event from the LED, regardless of whether a photon is detected or not. To ensure that the TAC is stopped by the correct reference signal—i.e., the one that follows the photon detection from the same excitation cycle—a deliberate delay is introduced to the reference pulse.

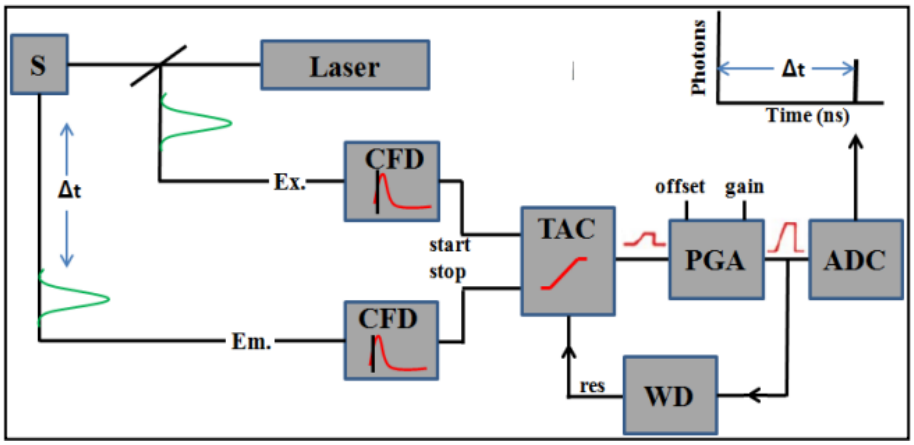

Figure 2.9 : Electronics module involved in TCSPC

The CFD precisely determines the arrival time of the photon and sends a signal to stop the voltage ramp in the TAC. The resulting voltage is directly proportional to the time delay (Δt) between the excitation and emission events. This analog voltage is then amplified using a Programmable Gain Amplifier (PGA) and subsequently converted into a digital value by an Analog-to-Digital Converter (ADC).

To maintain data accuracy, only voltage signals within a predefined range are accepted. A Window Discriminator (WD) filters out signals outside this range, thereby suppressing invalid events. The valid digital signal is then used to increment a specific memory location, effectively recording one photon detection event and its corresponding time delay. By repeating this process over many excitation cycles, a histogram of photon arrival times is built, representing the fluorescence decay curve of the sample.

2.3.4 Quantum Chemical Calculations

The ground-state geometries and molecular orbital distributions of the compounds were optimized using Density Functional Theory (DFT), applying the B3LYP exchange-correlation functional in combination with the 6-31G(d,p) basis set. To simulate solvent effects, the Polarizable Continuum Model (PCM) was employed throughout the calculations.

Excited-state energies, including those of the singlet (S_n) and triplet (T_n) states, were computed using Time-Dependent Density Functional Theory (TD-DFT) at the same level of theory. The energies of these excited states were determined by adding the calculated vertical excitation energies to the total energy of the optimized ground state.

All computations were performed using the Gaussian 16 software package on a high-performance workstation equipped with an Intel Xeon Silver 4208 processor (32 cores, 2.10 GHz clock speed, 16 threads) and 64 GB of RAM. Visualization of the frontier molecular orbitals was carried out using GaussView 6.0, while hole-electron analysis was conducted using the Multiwfn software suite.

Molecular docking simulations were conducted using the Schrödinger Suite 2014 installed on a Linux CentOS 6 platform, running on a 64-bit Intel® Core™ i5-2500 CPU @ 3.30 GHz with 4 GB of RAM. The docking workflow was carried out using the Maestro interface within the Schrödinger environment.

The synthesized ligand, RSM, was prepared using the LigPrep module, while the crystal structure of bovine serum albumin (BSA, PDB ID: 3V03) was pre-processed using the Protein Preparation Wizard. This involved the addition of hydrogen atoms, assignment of bond orders, optimization of hydrogen bonding networks, and energy minimization to ensure structural accuracy and stability.

Potential binding pockets on BSA were identified using the SiteMap tool, which locates druggable sites based on spatial and physicochemical criteria. For a site to be considered valid, a minimum of 15 site points was required. The analysis employed a stricter

definition of hydrophobicity and a standard grid spacing, with site boundaries trimmed to within 4 Å of the nearest site point.

Initial docking studies were performed to screen and rank potential binding sites on BSA based on estimated binding affinity. Glide was used in its extra precision (XP) mode to carry out these docking simulations. The scoring function used considers key interactions, including van der Waals forces, electrostatics, hydrogen bonding, and incorporates penalties for unfavorable interactions.

CHAPTER – 3
RESULT and DISCUSSION

Throughout this study, we have systematically investigated the photophysical behavior of RSM in various solvents. Detailed analysis of steady-state absorption, steady-state fluorescence, and time-resolved fluorescence (TRF) spectra indicates that RSM undergoes only intramolecular charge transfer (ICT), with no of other excited-state processes. Furthermore, concentration-dependent study in toluene, along with twisted intramolecular charge transfer (TICT) experiment in methanol–glycerol solvent system, confirm that RSM does not exhibit aggregation-induced emission (AIE) and that TICT is not operative under. Given that RSM is an oxazole derivative, therefore considering the known biological relevance of such compounds, we extended our study to probe its interaction with bovine serum albumin (BSA). Molecular binding studies revealed that RSM binds specifically to sodlow site I (subdomain IIA) of BSA.

3.1 Spectral characterization of RSM

The 1H NMR spectrum shown in Fig. 3.1 was obtained at 400 MHz spectrometer using DMSO-d6 solvent and tetramethylsilane (TMS) as an internal standard and the chemical shift was reported in ppm (ð). In the spectra triplet at 1.11 ppm and quartet at 3.5 ppm can be assigned to –CH3 and -CH2 protons respectively. Multiplet obtained in the region 6-8 ppm conferred to aromatic protons. Singlet peak present at 9.6 ppm can be attributed to phenolic -OH. Singlet peak present at 10.75 ppm can be attributed to phenolic -SO_3H.

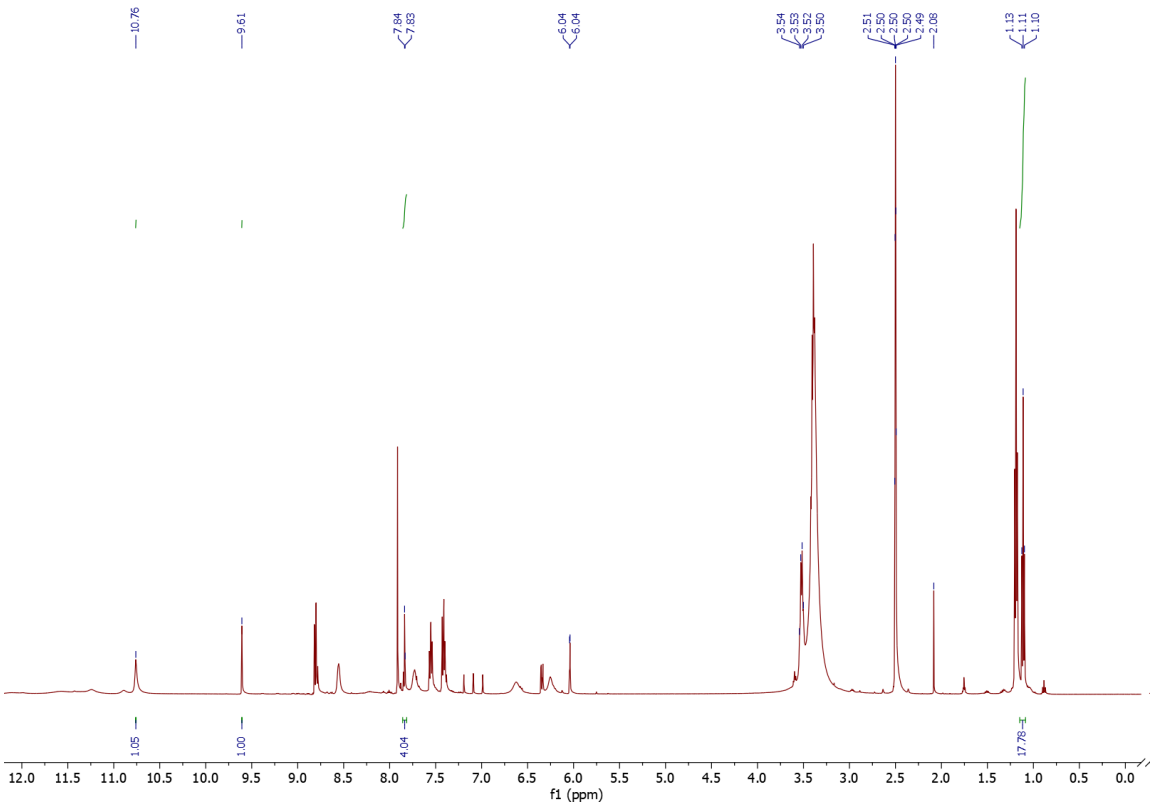

Fig. 3.1 : ^{1}H NMR spectrum of RSM.

3.2 Spectral Analysis of RSM in Different Solvents

A comprehensive study was performed on RSM (1mM) in various solvents ranging from non-polar toluene to polar aprotic acetonitrile (ACN) and highly polar protic water.

3.2.1 UV- Vis Absorption Study of RSM

The absorption spectra of RSM (Fig. 3.2) consistently showed a broad band between 480 and 590 nm, with a noticeable bathochromic (red) shift as solvent polarity increased. This shift highlights the sensitivity of RSM to its environment and suggests that the absorption arises from a π–π* electronic transition. The observed solvatochromism further supports the presence of an extended conjugated system in RSM, which interacts differently with solvents based on their polarity.

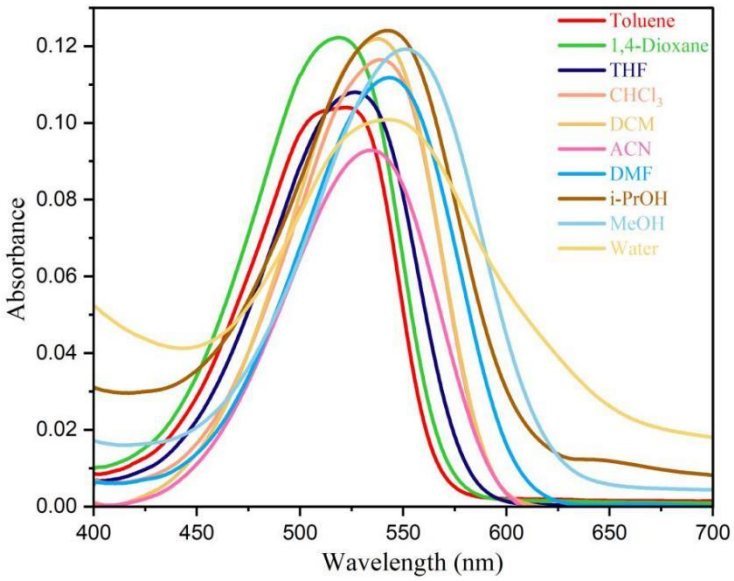

Fig 3.2 : Absorption spectra of RSM (1mM) in various solvents [298 K].

3.2.2 Steady State Fluorescence Emission Study of RSM

The emission properties of RSM were systematically investigated in solvents of varying polarity to understand its excited-state behavior. As illustrated in Fig. 3.5, the emission spectra displayed band spanning 540–640 nm, with a distinct bathochromic (red) shift observed upon increasing solvent polarity. Concurrently, a progressive decrease in fluorescence intensity was noted, culminating in complete quenching in water. This solvatochromic red shift indicates a significant difference in dipole moments between the ground and excited states, with the excited state exhibiting a higher polarity. The enhanced stabilization of the excited state in polar solvents lowers its energy, resulting in red-shifted emission. However, this stabilization also facilitate non-radiative deactivation pathways, thereby diminishing emission intensity. In highly polar protic solvents such as water, strong hydrogen bonding and solvent–solute interactions likely promote efficient internal conversion or intersystem crossing, leading to complete fluorescence quenching. These findings underscore the pronounced sensitivity of RSM's emissive state to solvent polarity and support the involvement of a highly polar, charge-transfer-type excited state. This observation is further supported by the analysis of the excited-state frontier molecular orbitals, as depicted in Fig. 3.3. The electron density distribution clearly

shows a shift from the diethylamine donor group toward the sulfonic acid acceptor moiety, thereby confirming the occurrence of intramolecular charge transfer (ICT) in the RSM molecule.

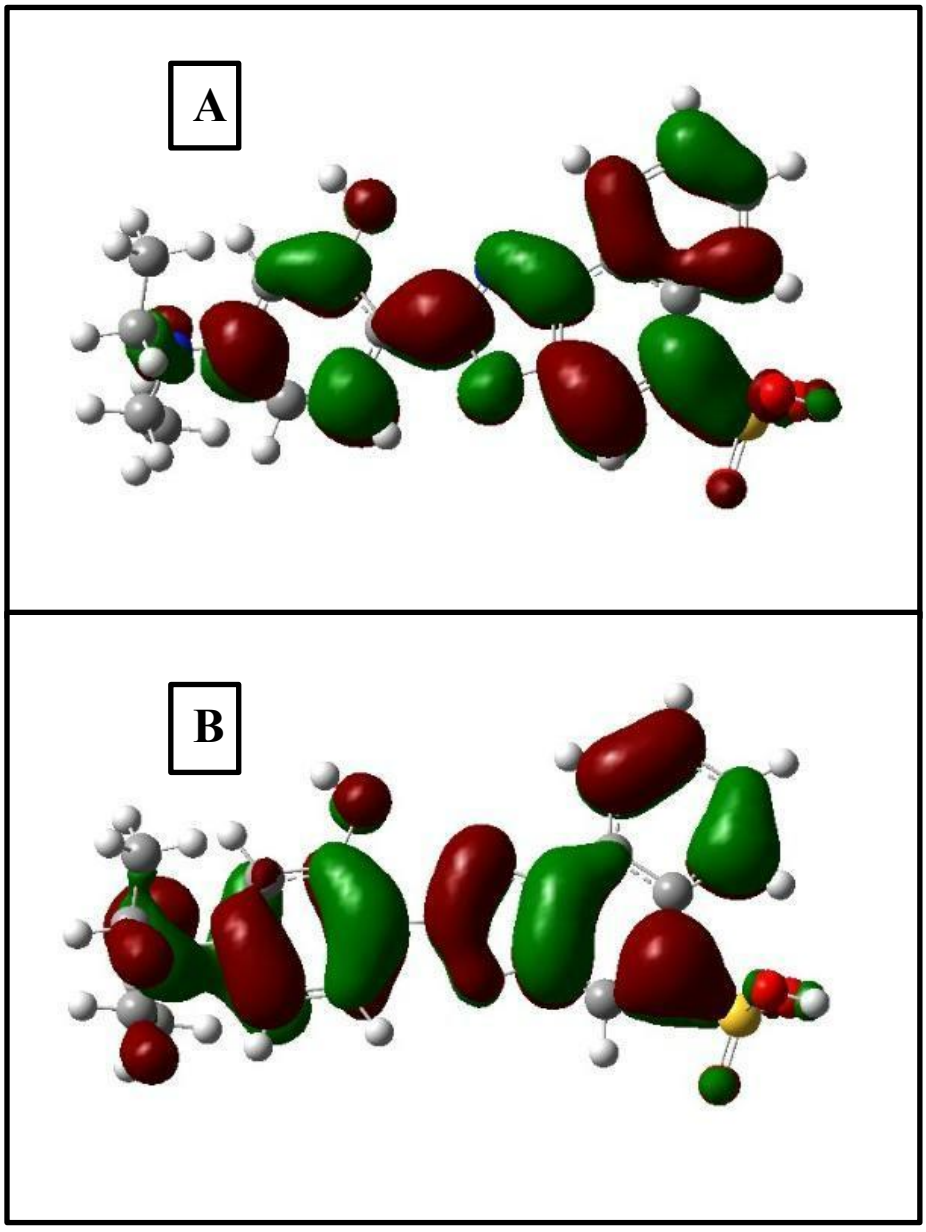

Fig 3.3 : Excited state molecular orbitals of RSM (A) LUMO (B) HOMO.

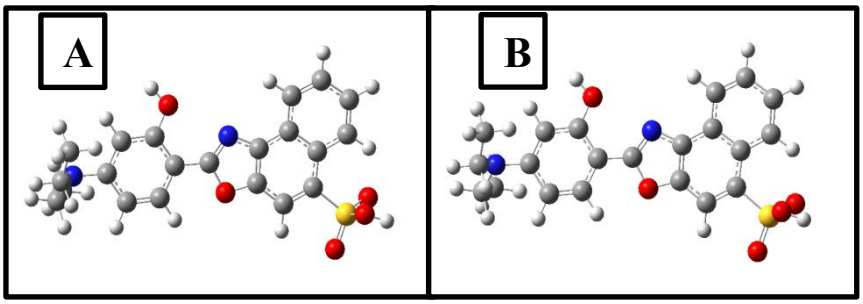

Fig 3.4 : Optimized structure of RSM (A) Ground state (B) Excited state.

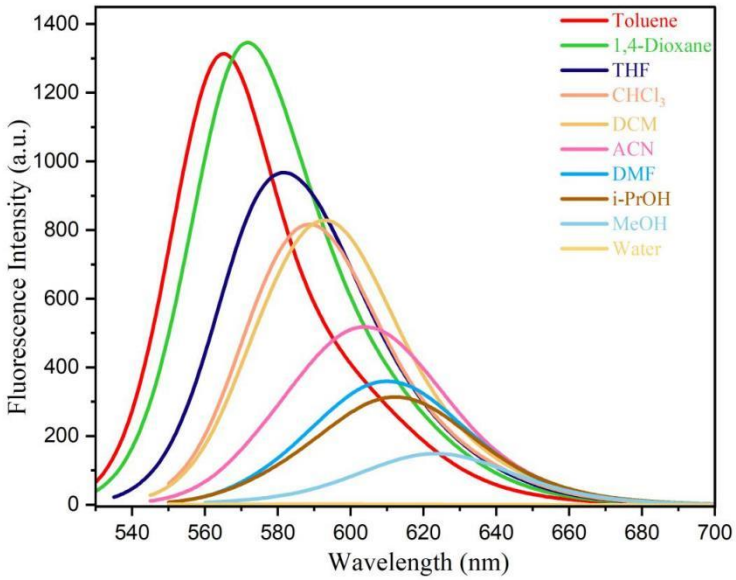

Fig 3.5 : Emission spectra of RSM (1mM mM) in various solvents [298 K].

Corresponding to the emission spectra the excitation spectra displayed 2 bands, one around 250 nm and the other around 500 nm as shown in Figure 3.6.

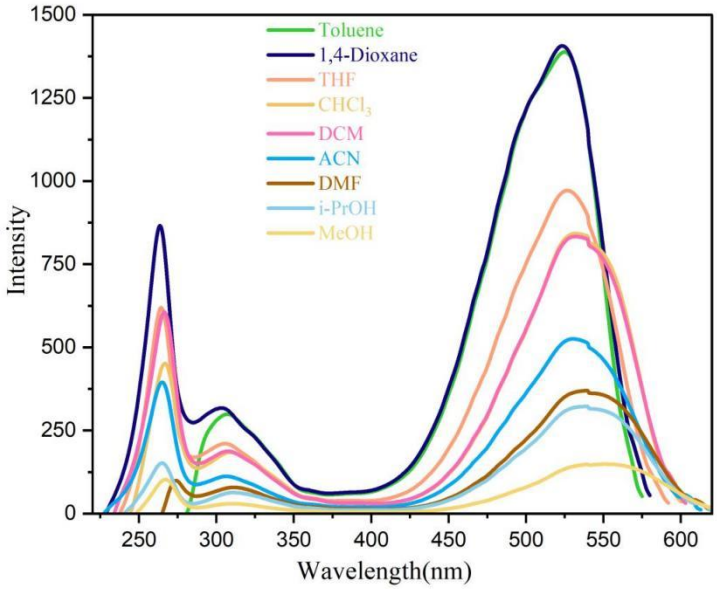

Fig 3.6 : Excitation spectra of RSM in various solvents [298 K].

The emission spectra of RSM for high energy peak is same as emission spectra of RSM as shown in Fig. 3.7.

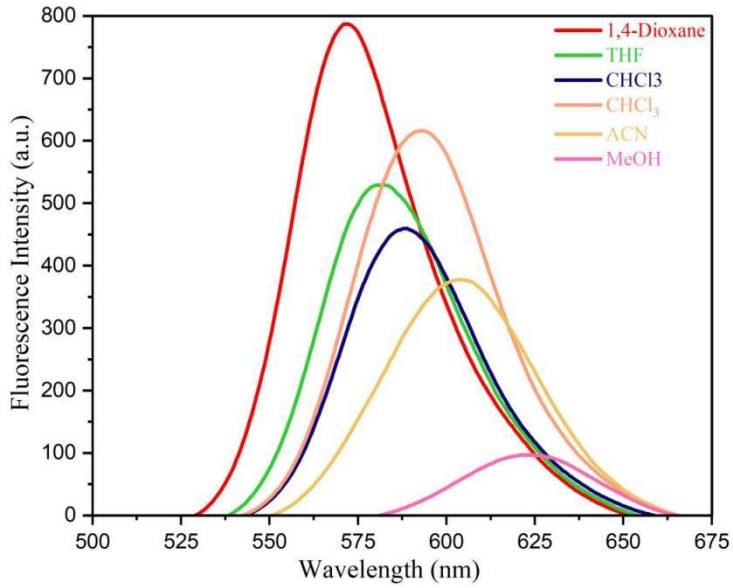

Fig 3.7 : Emission spectra of RSM in various solvents when excited at around 250nm [298K].

3.2.3 Time Resolved Fluorescence Emission Study of RSM

To gain deeper insights into the solvation dynamics of RSM, fluorescence lifetime measurements were conducted in various solvents at room temperature, with emission monitored at the respective maxima. The corresponding lifetimes are summarized in Table 1 and graphically represented in Fig. 3.8. The fluorescence decay profiles of RSM in all solvents were best fitted using a mono-exponential function, indicating a single dominant emissive species in each environment.

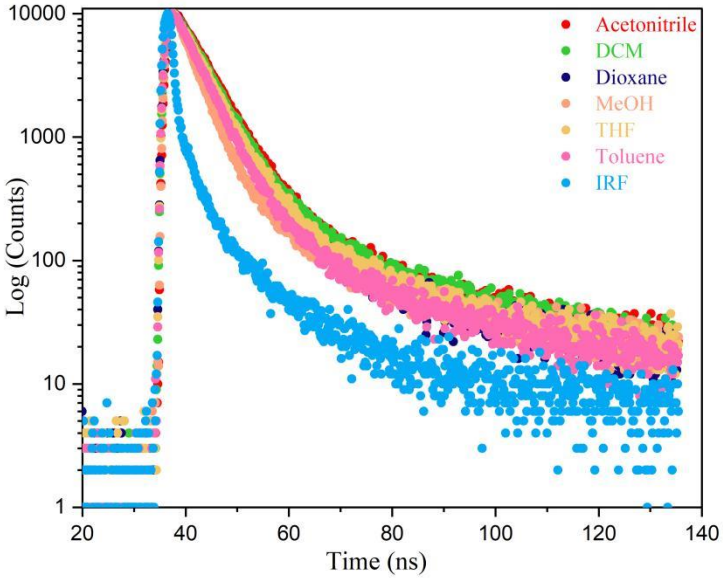

Fig 3.8 : Lifetime of RSM in Different Solvents.

Table 1 : Lifetime Data of RSM in different solvents

Solvent	τ_1 (ns)	α_1 %	τ_f (ns)	χ^2
Toluene	3.66	100	3.66	1.16
Dioxane	3.96	100	3.96	1.10
THF	4.15	100	4.15	1.18
DCM	4.43	100	4.43	1.31
ACN	4.58	100	4.58	1.29
MeOH	2.81	100	2.81	1.40

3.2.4 Concentration Dependent Study of RSM in Toluene

To further investigate the emission behavior, a concentration-dependent fluorescence study was conducted in toluene. The results showed a gradual increase in emission intensity with increasing concentration, reaching a saturation point at 120 µL as showed in Fig. 3.9. This behavior indicates that RSM does not exhibit aggregation-induced emission (AIE), confirming it is not an AIE-active compound.

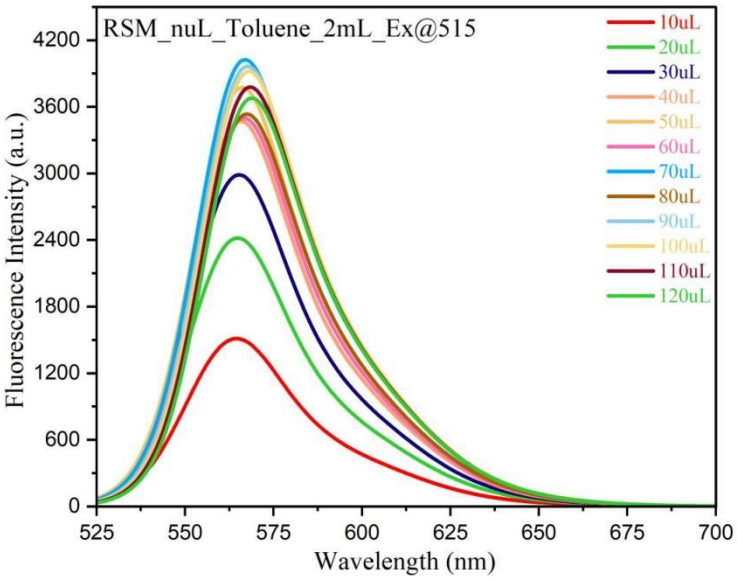

Fig 3.9 : Emission spectra of RSM in toluene when excited at around 250nm [298 K].

3.2.5 Test for Twisted Intramolecular Charge Transfer in RSM

To investigate the potential involvement of twisted intramolecular charge transfer (TICT) in RSM, fluorescence measurements were performed in a mixed solvent system of glycerol and methanol. As the proportion of glycerol increased, a slight red shift in the emission maximum along with a decrease in fluorescence intensity was observed as shown in Fig. 3.10. This trend is attributed to the increased polarity of glycerol, resulting in typical solvatochromic behavior rather than indicating the presence of a twisted

intramolecular charge transfer (TICT) state. These findings confirm that RSM does not exhibit TICT characteristics under these conditions.

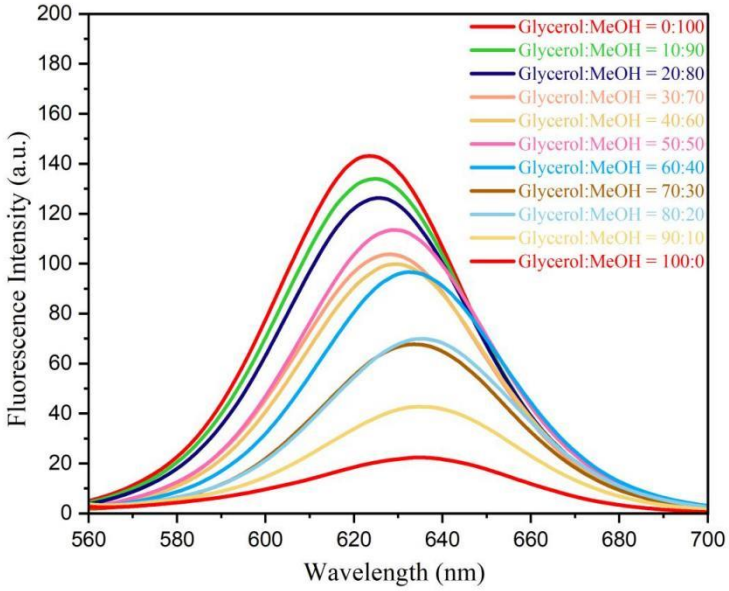

Fig 3.10 : Emission spectra of RSM in Glycerol - Methanol solvent system [298 K].

3.2.6 Naked Eye Visualization of Intramolecular Charge Transfer in RSM

A comprehensive photophysical investigation of RSM reveals that its excited-state behavior is predominantly governed by an intramolecular charge transfer (ICT) process. This ICT occurs from the electron-donating diethylamine group to the electron-withdrawing sulfonic acid moiety within the molecular framework. The strong push–pull electronic character of RSM facilitates efficient charge redistribution upon excitation, leading to significant changes in its spectral properties As the polarity of the solvent varies—from non-polar (e.g., toluene) to polar aprotic (e.g., acetonitrile) and polar protic (e.g., methanol or water). These observations are hallmarks of solvatochromism, a phenomenon wherein the spectral properties of a compound are modulated by its solvation environment.

The solvatochromic behavior of RSM is not only evident in its spectroscopic data but also visibly apparent to the naked eye. Distinct color changes in the solution are observed as the solvent polarity varies, reflecting the compound's sensitivity to its microenvironment. These visual cues, as captured in Fig. 3.11 and Fig. 3.12, further support the presence of strong ICT and highlight the potential of RSM as an environmentally responsive fluorescent probe.

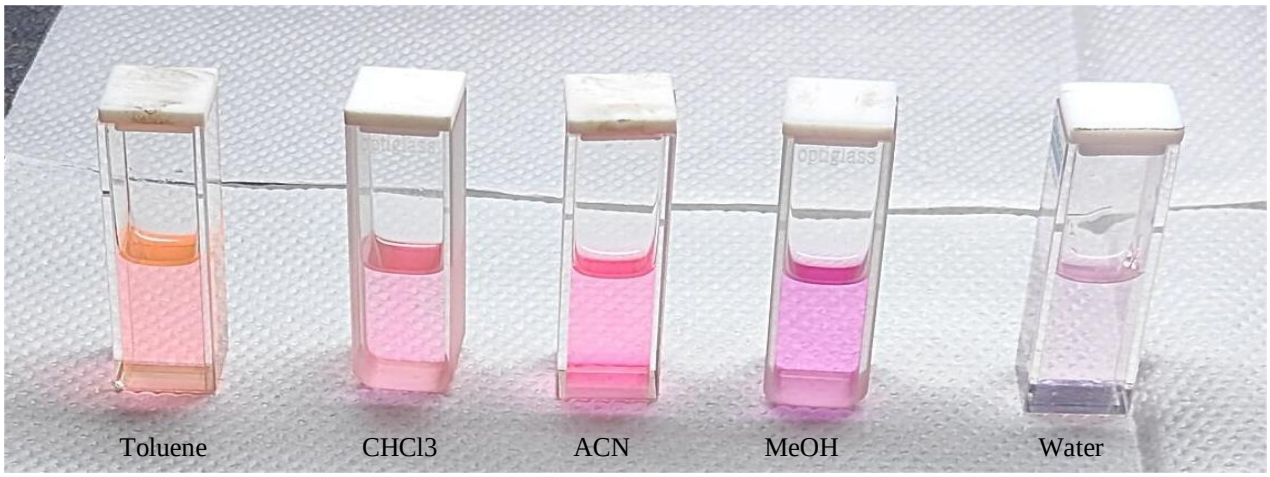

Fig 3.11 : RSM in different solvents under White Light.

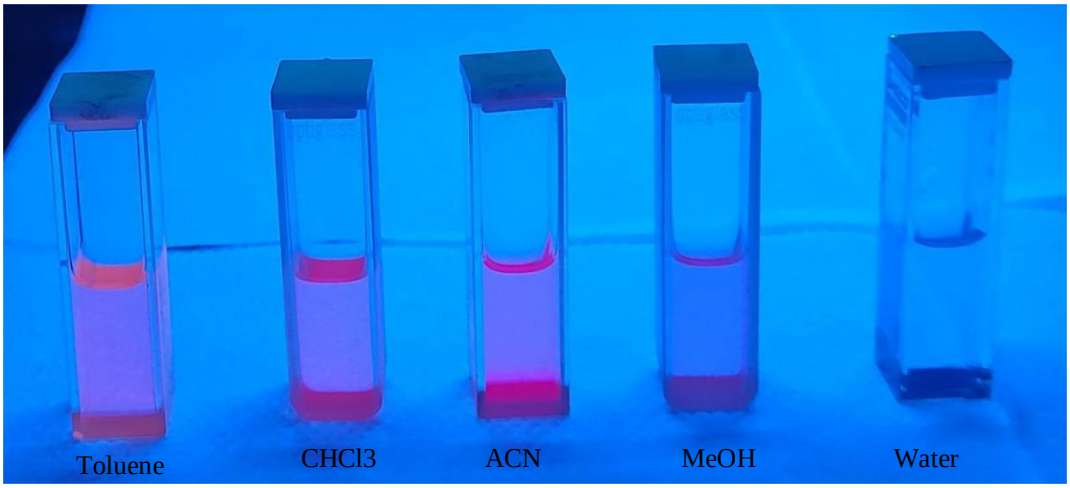

Fig 3.12 : RSM in different solvents under UV Light.

3.3 Elucidating the Binding Mechanism of RSM with Bovine serum Albumin (BSA) Through Spectroscopic and In Silico Approaches

3.3.1 Characterization of the RSM–BSA Interaction and Its Underlying Binding Mechanism

The interaction between RSM and bovine serum albumin (BSA) was explored by selectively exciting BSA's intrinsic tryptophan residues at 280 nm. In HEPES buffer at physiological pH (7.4), BSA displayed a characteristic fluorescence emission peak at 334 nm (Fig. 3.13). Upon gradual addition of RSM, a steady decline in fluorescence intensity at this wavelength was observed, along with a 14 nm blue shift in the emission maximum (Fig. 3.14). This blue shift implies that RSM does not disrupt the native fold of BSA. Normally, protein unfolding exposes Trp134 and Trp213 to the aqueous environment, resulting in a red shift in emission; however, the observed opposite effect suggests the tertiary structure remains intact.

Several processes can lead to fluorescence quenching, including excited-state interactions, conformational adjustments, energy transfer, and both dynamic and static quenching. These two latter mechanisms differ in their sensitivity to temperature and viscosity, and they can also be differentiated through fluorescence lifetime analysis. To determine the specific quenching mechanism responsible for RSM-induced fluorescence changes in BSA, a Stern–Volmer analysis was conducted using data collected at three different temperatures: 294 K, 298 K, and 304 K. The Stern–Volmer equation used for the analysis is as follows:

$$\frac{F_0}{F} = 1 + K_{sv}[Q] = 1 + K_q\tau_0[Q]$$

Where $\mathbf{F_0}$ and **F** represent the fluorescence intensities of BSA in the absence and presence of the quencher (RSM), respectively; $\mathbf{K_{sv}}$ is the Stern–Volmer quenching constant; **[Q]** is the quencher concentration; $\mathbf{K_q}$ is the bimolecular quenching rate constant; $\boldsymbol{\tau_0}$ is the average fluorescence lifetime of BSA in the absence of the quencher.

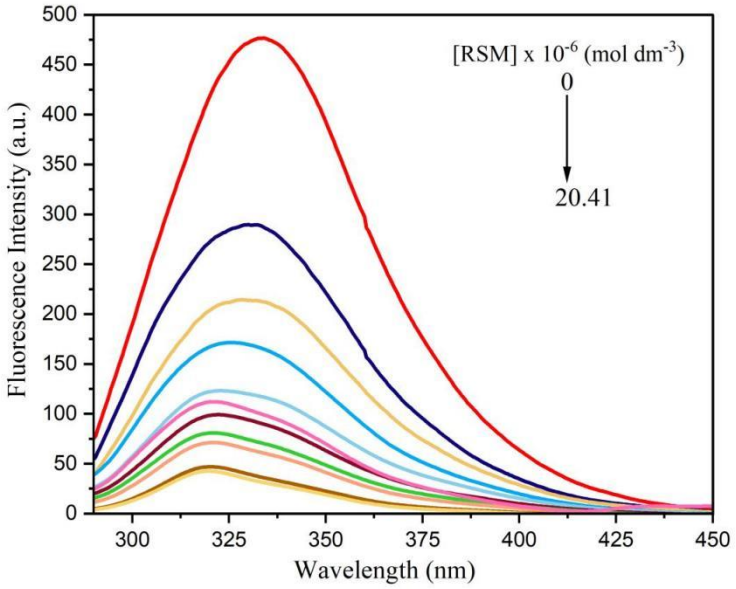

Fig 3.13 : Emission spectra showing quenching of BSA tryptophan fluorescence with increasing RSM concentration at 294 K.

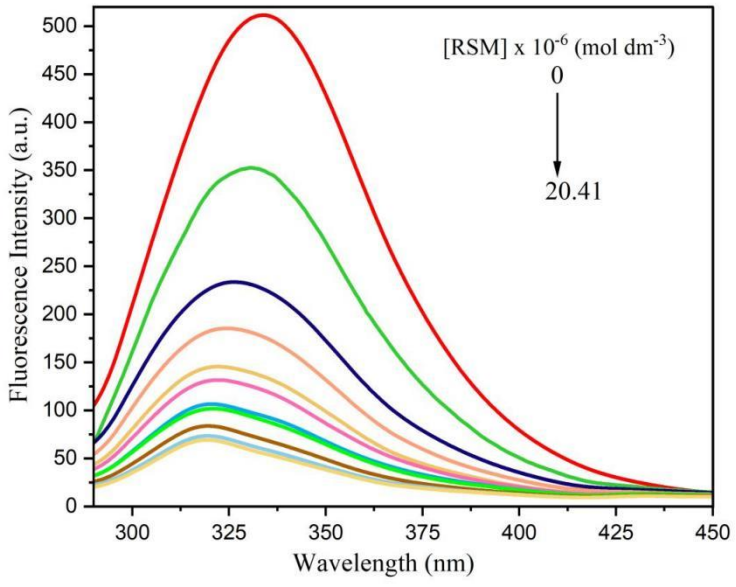

Fig 3.14 : Emission spectra showing quenching of BSA tryptophan fluorescence with increasing RSM concentration at 298 K.

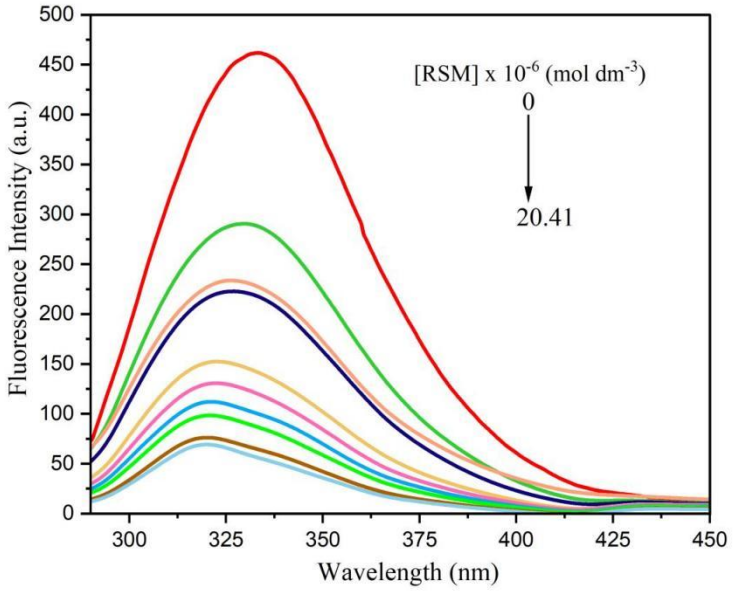

Fig 3.15 : Emission spectra showing quenching of BSA tryptophan fluorescence with increasing RSM concentration at 304 K.

The Stern–Volmer plot for the RSM–BSA system (Fig. 3.16) exhibited a linear trend, indicative of a static quenching mechanism. As detailed in Table 2, the Stern–Volmer quenching constant (Ksv) showed a gradual decline with rising temperature, further confirming the static nature of the interaction. The bimolecular quenching rate constant (Kq) was estimated using the average fluorescence lifetime of native BSA (τ_0) in the absence of RSM. The resulting Kq values exceeded the diffusion-limited quenching constant typically associated with dynamic quenching in biomolecular systems (approximately 2.0×10^{10} L mol^{-1} s^{-1}). This significant deviation suggests that the quenching arises not from transient collisional encounters but rather from stable ground-state complex formation—hallmarks of static quenching.

Moreover, the temperature-dependent decline in Ksv values implies a moderately strong interaction between RSM and BSA. Such moderate binding affinity may offer pharmacokinetic advantages, potentially allowing RSM to bind reversibly to serum albumin and be gradually released to reach target tissues more efficiently.

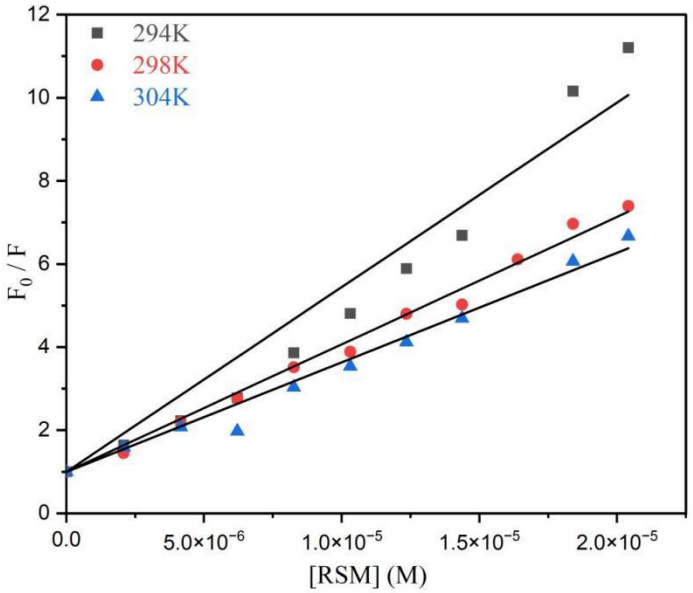

Fig 3.16 : Stern–Volmer plots at varying temperatures Depicting the quenching interaction between RSM and BSA.

Table 2 : Quenching parameters of RSM-BSA interaction at various temperatures.

T (K)	K_{sv} (10^{12} $Lmol^{-1}S^{-1}$)	K_q (10^{12} $Lmol^{-1}S^{-1}$)	R^2
294	44.43 ± 2.18	14.13 ± 0.22	0.98
298	30.66 ± 0.51	9.75 ± 0.051	0.99
304	26.34 ± 0.73	8.38 ± 0.073	0.99

To further elucidate the exact quenching mechanism in both cases, time-resolved fluorescence (TRF) analysis was also employed (see below). For static quenching interactions, the binding constant and the number of binding sites can be determined using the double-logarithmic equation as shown.

$$\log\left(\frac{F_0 - F}{F}\right) = \log K_b + n\log[Q]$$

Where F_0 and F are the fluorescence intensities in the absence and presence of RSM, respectively. According to the equation above, if a plot of log((F₀ - F) / F) versus log [Q] yields a straight line, the slope corresponds to the binding site number "n." As shown in Fig. 3.17, the linear relationship and the value of "n" close to 1 for the RSM–BSA interaction indicate the presence of a single binding site. The binding constant (K_b) for the RSM–BSA interaction is calculated to be 13.0×10^5 M^{-1}, reflecting a moderate to strong binding affinity when compared to protein-ligand complexes with higher binding constants (10^6 – 10^8 M^{-1}). This moderate K_b value provides valuable insight into the potential therapeutic effectiveness of RSM.

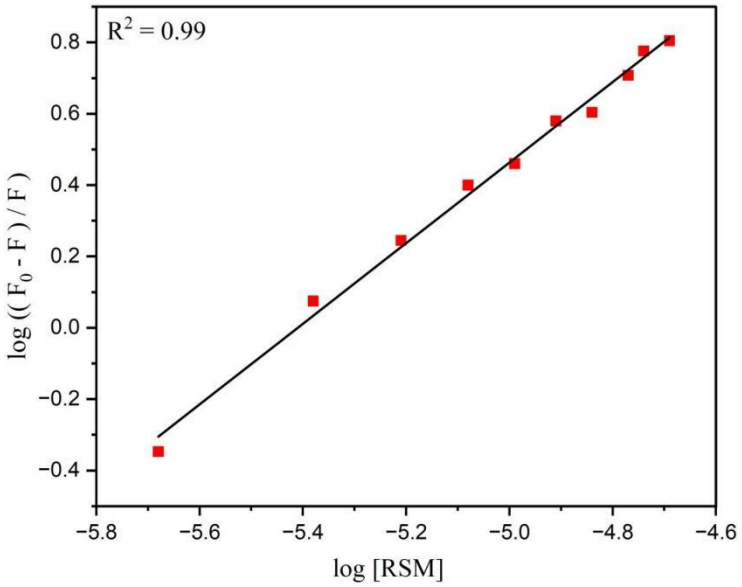

Fig 3.17 : Double logarithmic plot for binding affinity between RSM and BSA.

3.3.2. Thermodynamic Analysis of the RSM–BSA Binding Interaction

Non-covalent forces such as hydrogen bonding, van der Waals interactions, hydrophobic contacts, and electrostatic attractions mainly govern ligand–protein associations. As described by Ross and Subramanian, analyzing the sign and magnitude of thermodynamic parameters—enthalpy change (ΔH) and entropy change (ΔS)—offers insight into the dominant forces contributing to binding. If the temperature variation

across experiments is relatively narrow, ΔH is often assumed to remain constant within that range. Under such circumstances, both ΔH and ΔS can be determined using the van't Hoff equation:

$$\ln K = -\frac{\Delta H}{RT} + \frac{\Delta S}{R}$$

Here, K represents the effective association constant (K_a) at a given temperature, R is the universal gas constant, and T denotes the absolute temperature in Kelvin.

In this investigation, a modified Stern–Volmer method was utilized to determine the association constant (K_a) values for the RSM–BSA complex across different temperatures.

$$\frac{F_0}{\Delta F} = \frac{1}{f_a K_a [Q]} + \frac{1}{f_a}$$

The calculated association constants (K_a), with correlation coefficients of 0.99 (Fig. 3.18), are summarized in Table 3. The K_a values were in the range of 10^4, indicating a moderate binding affinity between RSM and BSA.

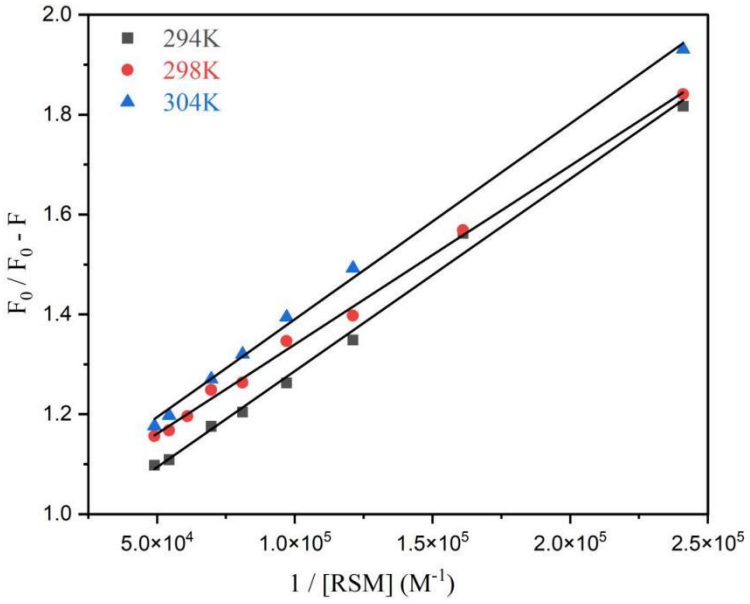

Fig 3.18 : Modified Stern–Volmer plots at different temperatures illustrating the interaction between RSM and BSA.

A linear relationship observed in the van't Hoff plot of $\ln K_a$ versus 1/T (Fig. 3.19) confirmed that ΔH remained approximately constant across the temperature range investigated. From the slope and intercept of the plot, ΔH and ΔS were obtained, respectively. Additionally, the Gibbs free energy change (ΔG) at each temperature was calculated using the following equation:

$$\Delta G = \Delta H - T\Delta S = -RT\ln K$$

For the RSM–BSA interaction, the thermodynamic parameters were found to be ΔH < 0 (very small negative) and ΔS > 0 (Table 3), indicating that electrostatic interactins were the primary driving forces for binding. In some extent hydrogen bonding and van der Waals interactions were also present. The negative ΔG values at all studied temperatures further confirmed the spontaneous nature of the quenching process. Thus, the combination of negative ΔH and positive ΔS supports a favorable, spontaneous interaction between RSM and BSA.

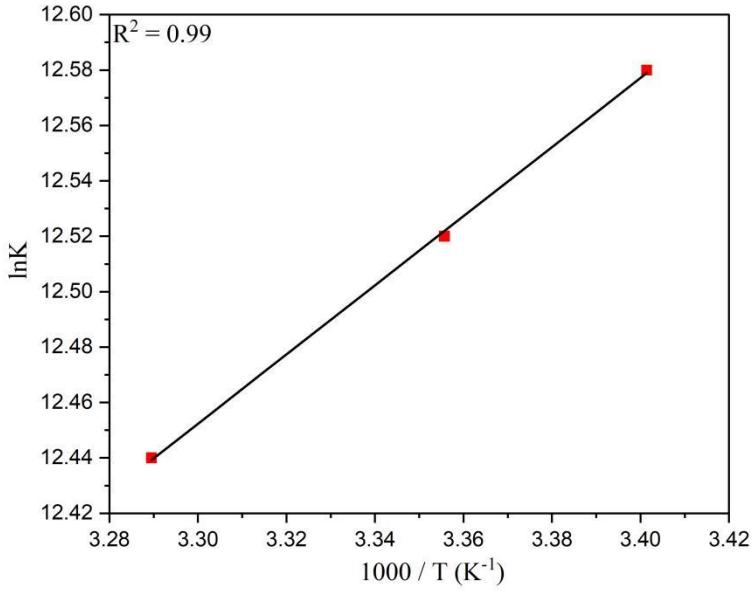

Fig 3.19 : Van't Hoff plots illustrating the temperature dependent binding behavior between RSM and BSA.

Table 3 : Temperature-Dependent Thermodynamic Parameters for the RSM–BSA System

T(K)	Ka (10^4 $Lmol^{-1}$)	ΔH ($kJmol^{-1}$)	ΔG ($kJmol^{-1}$)	ΔS ($JK^{-1}mol^{-1}$)	R^2
294	23.41 ± 0.82		-20.80		
298	27.45 ± 0.62	-0.145	-21.12	70.37	0.99
304	27.45 ± 0.62		-21.50		

3.3.3 Dynamics of the Excited State

Fluorescence lifetimes are a sensitive measure for probing the local environment of a fluorophore and are crucial for understanding interactions between probes and proteins. Time-resolved fluorescence (TRF) measurements were used to examine the blue shift and the quenching mechanism of tryptophan fluorescence both in the absence and presence of RSM. The decay profiles for free BSA and RSM-bound BSA are shown in Fig. 3.20. BSA typically exhibits a bi-exponential decay pattern. The longer lifetime component (Table 4) is attributed to the water-exposed Trp134, while the shorter component corresponds to the buried Trp213, consistent with previous studies.

In this study, the average fluorescence lifetime of BSA τ_f was analyzed to evaluate its interaction with RSM, as summarized in Table 3. Rather than emphasizing the individual decay components, τ_f was selected as a representative parameter to assess the overall quenching behavior. In the absence of RSM the average lifetime of BSA was found to be 3.18 ns. Upon incremental addition of RSM, a gradual decrease in τ_f was observed, reaching 1.83 ns at a concentration of 20.41 μM. This moderate decrease in lifetime suggests the involvement of dynamic quenching to a minor extent.

Additionally, analysis of the relative amplitude contributions revealed significant changes with increasing RSM concentration. The fractional contribution of the faster decay component α_1 increased from 61.72% (in the absence of RSM) to 84.19% at 20.41

μM RSM. In contrast, the contribution of the slower decay component α_2 decreased from 38.28% to 15.81% over the same concentration range. These systematic shifts in amplitude distribution imply that RSM induces conformational or microenvironmental changes in the vicinity of BSA's tryptophan residues. This perturbation is further supported by the alterations observed in the three-dimensional fluorescence spectral profiles, indicating a possible reorganization of the protein's tertiary structure upon interaction with RSM.

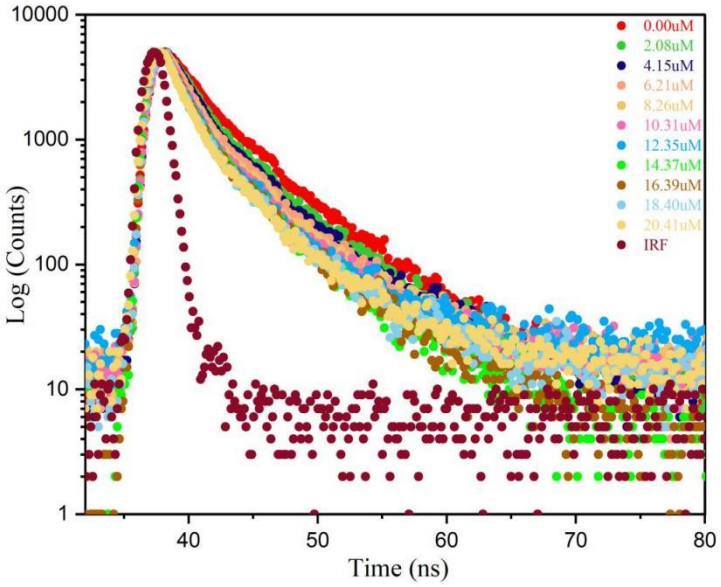

Fig 3.20 :Time-Resolved Fluorescence Decay of BSA upon Increasing [RSM] at 298 K. Excitation at 280 nm, Emission at 330 nm, pH 7.4.

Table 4 : Lifetime Data for Varying [RSM] in the Environment of BSA at 298 K, P^H 7.4.

[RSM](uM)	τ_1 (ns)	τ_2 (ns)	α_1 %	α_2 %	τ_f (ns)	χ^2
0.0	1.84	5.34	61.72	38.28	3.18	1.56
2.08	1.67	5.06	70.41	29.59	2.67	1.15
4.15	1.52	5.14	75.07	24.93	2.43	1.92
6.21	1.69	5.24	80.99	19.01	2.36	1.53
8.26	1.68	5.15	82.00	18.00	2.30	1.45
10.31	1.35	4.51	78.92	21.08	2.02	1.46
12.35	1.65	5.30	88.81	11.19	2.06	1.45
14.37	1.50	4.88	83.46	16.54	2.06	1.13
16.39	1.28	4.38	80.27	19.73	1.89	1.15
18.40	1.23	4.55	82.55	17.45	1.81	1.41
20.41	1.30	4.64	84.19	15.81	1.83	1.03

3.3.4 Identification of RSM binding site in bovine serum albumin protein

Understanding the binding site of RSM on BSA is essential for determining its free and bound forms, as competition for binding sites on BSA may influence these forms. Sudlow et al. identified two primary binding sites on the protein: Site I (subdomain IIA) and Site II (subdomain IIIA). Site I binds compounds like Warfarin and phenylbutazone, while Site II has a preference for Ibuprofen and flufenamic acid. To explore this, competitive binding experiments were performed where RSM was titrated into a BSA solution along with typical site markers (Warfarin and Ibuprofen) in a 1:1 ratio ([BSA]:[site marker]). During the competitive binding process, both the compound and site marker compete for the same binding site, and changes in the fluorescence intensity can be used to evaluate the extent of binding interaction. The quenching pattern of BSA fluorescence upon the addition of Warfarin and RSM (Fig. 3.21) shows a similar trend,

suggesting competition between the two, while a different quenching pattern is observed for Ibuprofen and RSM (Fig. 3.22).

To compare the effects of Warfarin and Ibuprofen on RSM binding to BSA, a modified Stern-Volmer approach (Fig. 3.23) was utilized, and the association constants (Ka) of the bichromophoric compound in the absence and presence of site markers were calculated (Table 5). The Ka value for the RSM-BSA complex is $(27.74 \pm 0.1) \times 10^4\ M^{-1}$, while in the presence of Warfarin and Ibuprofen, the values are $(20.50 \pm 37.64) \times 10^4\ M^{-1}$ and $(13.79 \pm 11.98) \times 10^4\ M^{-1}$, respectively. These results indicate competition between RSM and Warfarin, suggesting that RSM binds to Site I of subdomain IIA on BSA, the same site where Warfarin binds.

This competitive interaction is further corroborated by time-resolved fluorescence data, including lifetime and percentage contribution, as shown in Tables 6 and 7, and Figures 3.24 and 3.25.

Table 5 : Parameters of Competitive Site Replacement Experiments at 298 K for RSM Binding to BSA.

Site marker	$K_a \times (10^4\ M^{-1})$	R^2
Blank	27.74 ± 0.1	0.99
Warfarin	20.50 ± 0.1	0.99
Ibuprofen	13.74 ± 11.98	0.94

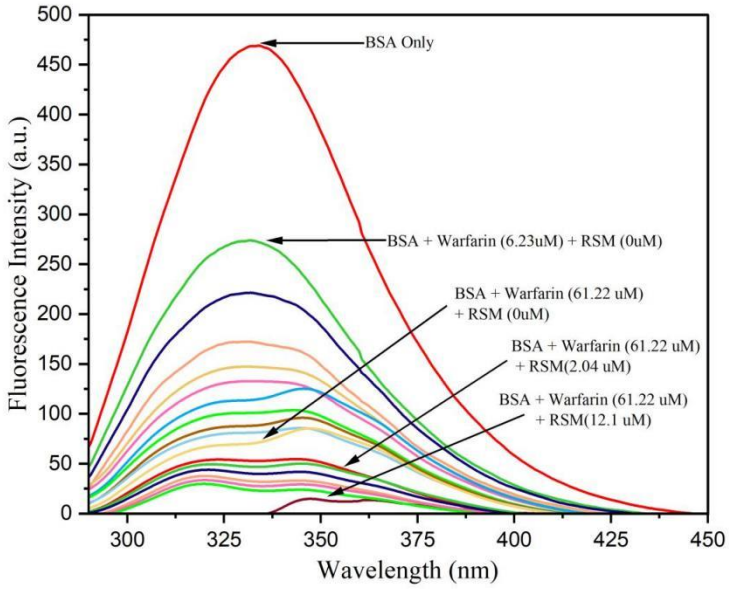

Fig 3.21 : Fluorescence Emission Profiles of BSA with Warfarin and RSM at 298 K.

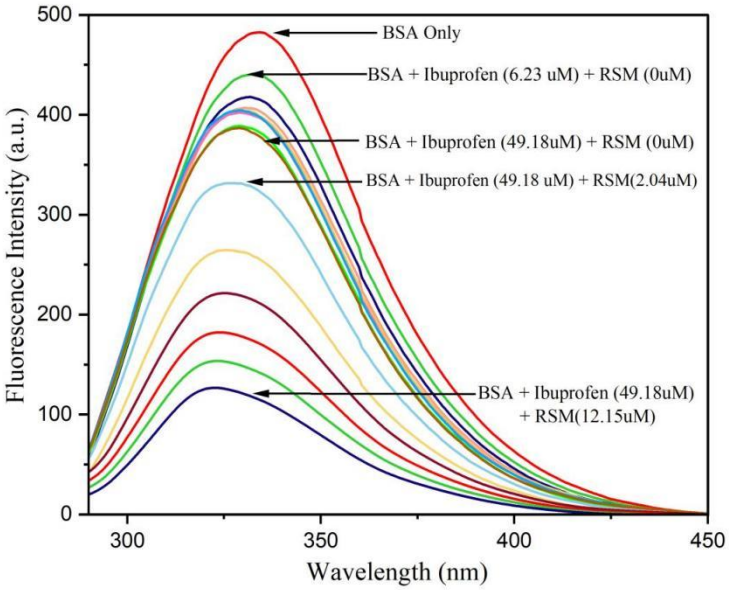

Fig 3.22 : Fluorescence Emission profiles of BSA with Ibuprofen and RSM at 298K.

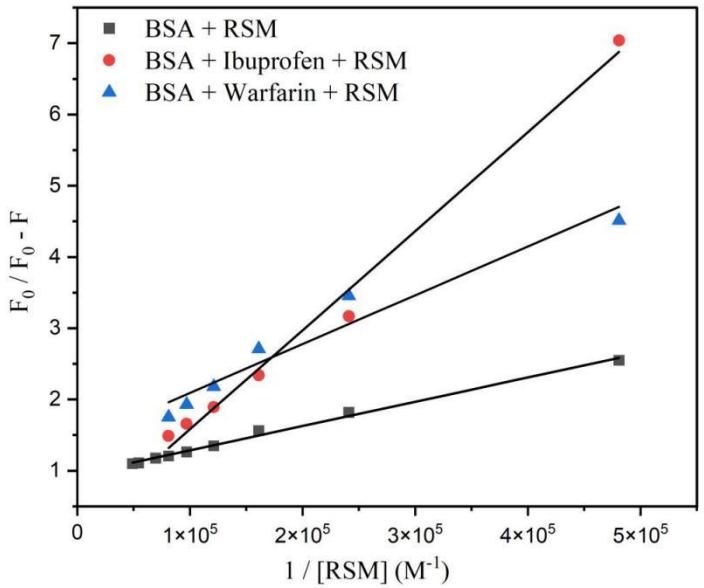

Fig 3.23 : Modified Stern–Volmer plots illustrating the binding interaction of RSM with BSA in the absence and presence of site-specific probes Ibuprofen and Warfarin at 298 K.

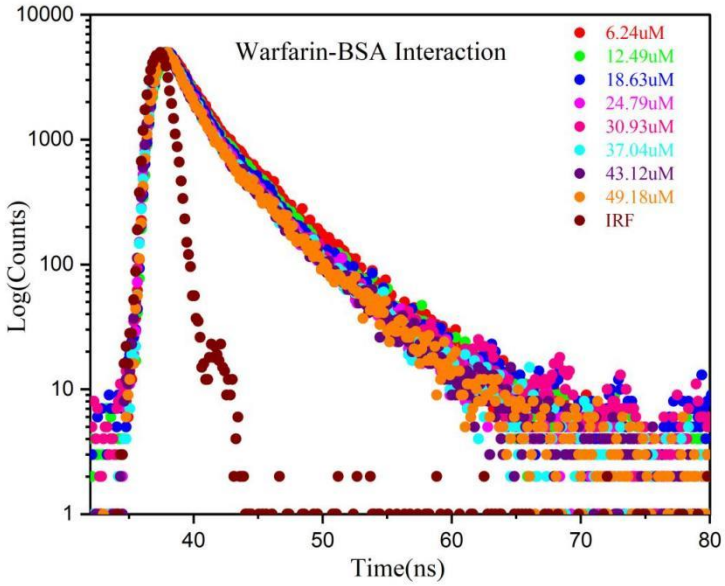

Fig 3.24 : Time-resolved fluorescence decay of BSA with increasing [Warfarin] at 298 K.

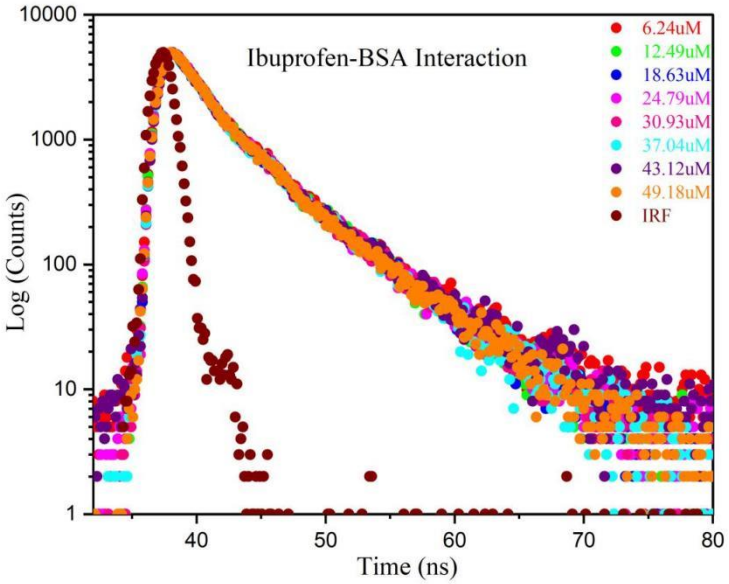

Fig 3.25 : Fluorescence decay profiles of BSA at 298 K showing Variation with increasing concentrations of Warfarin.

Table 6 : Lifetime Data for varying [Warfarin] in the Environment of BSA at 298 K, P^H 7.4.

[Warfarin](uM)	τ_1 (ns)	τ_2 (ns)	α_1 %	α_2 %	τ_f (ns)	χ^2
0.0	1.94	5.47	68.03	31.97	3.07	1.62
6.24	1.50	4.45	68.11	31.89	2.44	1.17
12.49	1.13	3.81	62.30	37.70	2.14	1.75
18.63	1.46	4.35	74.31	25.69	2.20	1.25
24.79	1.58	4.68	80.00	20.00	2.20	1.09
30.93	1.49	4.50	79.50	20.51	2.10	1.39
37.04	1.52	4.58	80.72	19.28	2.11	1.30
43.12	1.49	4.48	80.49	19.51	2.07	1.11
49.18	1.46	4.51	82.20	17.80	2.00	1.05

Table 7 : Lifetime Data for Increasing [Ibuprofen] in the BSA Environment at 298 K, P^H 7.4.

[Ibuprofen](uM)	τ_1 (ns)	τ_2 (ns)	α_1 %	α_2 %	τ_f (ns)	χ^2
0.0	1.94	5.47	68.03	31.97	3.07	1.62
6.24	1.70	5.07	64.32	35.68	2.91	1.59
12.49	1.84	5.50	70.29	29.71	2.93	1.17
18.63	1.91	5.51	71.21	28.79	2.95	1.25
24.79	1.82	5.51	71.50	28.50	2.87	1.61
30.93	1.64	5.30	69.45	30.55	2.76	1.23
37.04	1.62	5.07	65.74	34.26	2.80	1.24
43.12	1.83	5.32	69.05	30.95	2.91	1.66
49.18	2.15	5.78	75.48	24.52	3.04	1.39

3.3.5 3D Fluorescence Spectral Analysis of RSM–BSA Interaction

In the 3D fluorescence spectra, peak a (where $\lambda ex = \lambda em$) corresponds to Rayleigh scattering. In addition, two significant fluorescence peaks are observed: peak 1 at an excitation wavelength of 285 nm and peak 2 at 240 nm. Peak 1 is attributed to the intrinsic fluorescence of tryptophan residues in bovine serum albumin (BSA), reflecting changes in the protein's tertiary structure. Peak 2 is associated with alterations in the secondary structure of the protein. Upon the stepwise addition of RSM, a progressive decrease in fluorescence intensity is noted for both peaks as shown in Fig. 3.25 and 3.26. This reduction indicates that RSM interacts with BSA, inducing microenvironmental changes that result in subtle modifications to both the peptide backbone (secondary structure) and the overall tertiary structure of the protein.

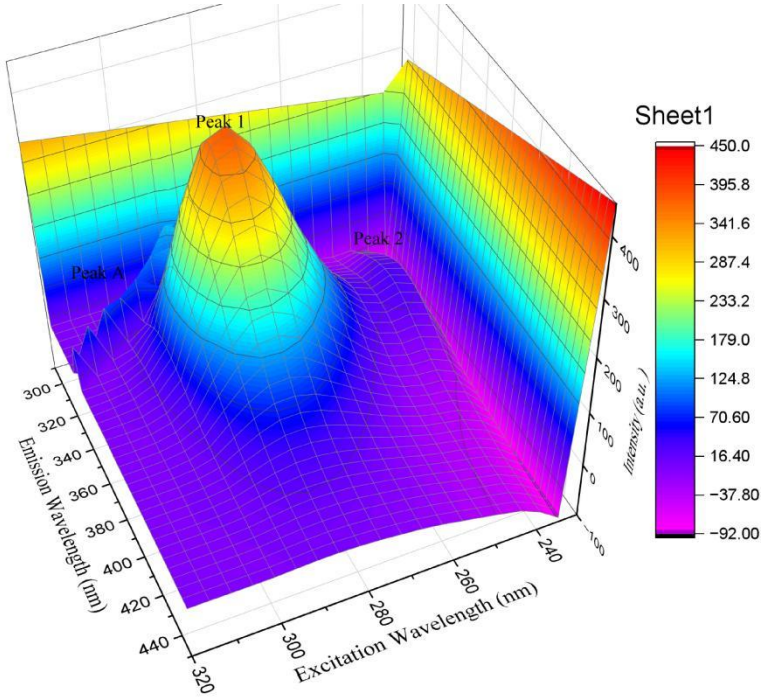

Fig 3.26 : 3D Fluorescence spectra of BSA only.

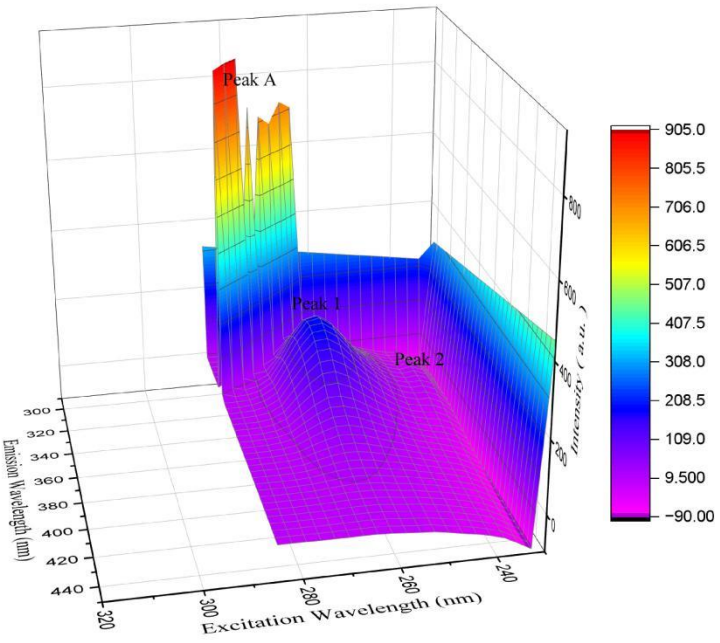

Fig 3.27 : 3D Fluorescence spectra of RSM- BSA.

3.3.6 In Silico Exploration of Amino Acid Residues Near the Binding Site

To gain a detailed understanding of the binding conformation and preferred interaction site of RSM on BSA, and to support the experimental spectroscopic results, a computational approach was adopted. This included the application of molecular docking to systematically explore the site-specific interaction between RSM and BSA.

The spatial orientation and interaction pattern of small molecules within bovine serum albumin (BSA) critically influence their pharmacological behavior under physiological conditions. BSA possesses two main ligand-binding cavities located in subdomains IIA and IIIA, corresponding to Sudlow's site I and II, respectively. To pinpoint the binding mode and preferred site of RSM, molecular docking was performed using the crystal structure of BSA (PDB ID: 3VO3) via the Glide docking module.

The docking analysis demonstrated that RSM preferentially binds within subdomain IIA—Sudlow site I—with a notable docking score of –7.3, indicating a strong binding affinity. Within this site, RSM participates in π–π stacking interactions with the HIE145 residue, forms a hydrogen bond with SER428, and engages in π–cation interactions with ARG458. This pocket, commonly referred to as the "warfarin binding site," is lined with several hydrophobic amino acid residues that facilitate stable ligand accommodation through nonpolar interactions (visualized in Fig. 3.28).

These computational results are consistent with the experimental displacement studies and support the spectroscopic observations, including the blue shift in emission and thermodynamic evidence. The combined findings highlight that hydrophobic interactions predominantly drive the formation of the RSM–BSA complex, reinforcing the proposed binding mechanism.

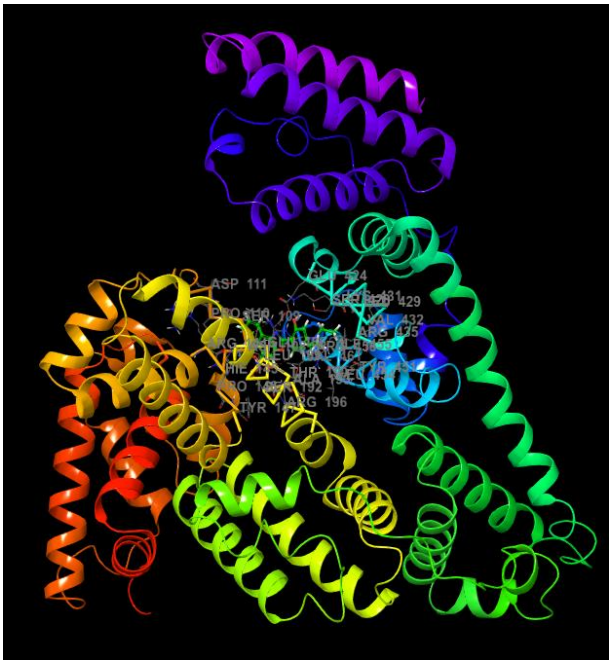

Fig 3.27 : Lowest-energy binding conformation of RSM positioned within the hydrophobic cavity of Sudlow site I (subdomain IIA) of BSA (PDB ID: 3VO3).

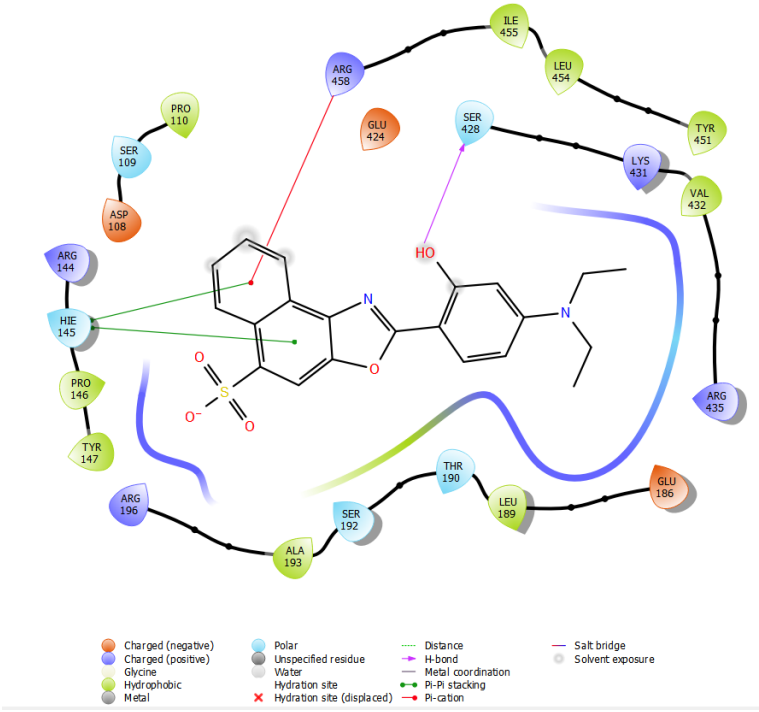

Fig 3.28 : 2D Interaction Map Depicting Key Residue Contacts Stabilizing RSM within the BSA Binding Pocket

CHAPTER-4
CONCLUSION and FUTURE PLANS

4.1 Conclusion

Overall, the study provides the design and synthesis of novel oxazole derivative (cyclized schiff base) 2-(4-(diethylamino)-2-hydroxyphenyl)naphtho[1,2-d]oxazole-5-sulfonic acid (RSM). RSM is characterized using ^{1}H NMR spectroscopy. Comprehensive spectral analysis of RSM using UV-Vis absorption spectroscopy, steady state fluorescence emission spectroscopy, and time resolved fluorescence emission spectroscopy in various solvents exhibits a strong intramolecular charge transfer (ICT) behavior, which is solvent-polarity dependent, as evidenced by a bathochromic shift in both absorption and emission spectra. The decrease in fluorescence intensity with increasing solvent polarity and complete quenching in water indicates non-radiative decay in polar protic media. Fluorescence lifetime measurements further supported these findings. Mono-exponential decay was observed across all solvents, suggesting a single emissive species. Lifetimes increased from 3.66 ns (toluene) to 4.58 ns (acetonitrile), while in methanol the lifetime dropped to 2.81 ns, highlighting the role of solvent polarity and hydrogen bonding in modulating the excited-state dynamics. Concentration-dependent studies in toluene showed minimal changes in emission characteristics, indicating no aggregation-induced emission (AIE). Similarly, viscosity-dependent fluorescence in methanol–glycerol mixtures excluded the presence of twisted intramolecular charge transfer (TICT). Molecular orbital analysis confirmed effective intramolecular charge transfer, with HOMO localized on the diethylamino donor and LUMO on the sulfonic acid acceptor.

Naked-eye observations under white and UV light further corroborated spectroscopic data. Under white light, RSM solutions exhibited visible color changes from yellow to reddish hues depending on solvent polarity. Under UV light (365 nm), strong

fluorescence was observed in non-polar solvents, gradually diminishing with increasing polarity and completely quenched in water.

The interaction between RSM and bovine serum albumin (BSA) was systematically investigated using steady-state fluorescence, time-resolved fluorescence spectroscopy, and molecular docking. Fluorescence titration experiments demonstrated progressive quenching of BSA's intrinsic tryptophan fluorescence with increasing RSM concentration, accompanied by a 14 nm blue shift (from 334 to 320 nm), indicating RSM is interacting with a more hydrophobic region of BSA. Stern–Volmer analysis indicated a predominantly static quenching mechanism, supported by decreasing quenching constants (K_{sv}) with rising temperature: 44.43×10^{12}, 30.66×10^{12}, and 26.34×10^{12} $Lmol^{-1}s^{-1}$ at 294 K, 298 K, and 304 K, respectively. Time-resolved measurements showed a moderate decrease in BSA's average lifetime from 3.18 ns to 1.83 ns at 20.41 μM RSM, suggesting a minor dynamic quenching contribution.

The static binding constant and number of binding sites were determined to be 1.30×10^{6} M^{-1} and approximately 1, indicating moderate to high binding affinity. Thermodynamic parameters derived from van't Hoff analysis ($\Delta H = -0.145$ $kJ \cdot mol^{-1}$ and $\Delta S = 70.37$ $J \cdot K^{-1} \cdot mol^{-1}$) suggested that electrostatic interactions predominantly drive the binding process, with additional contributions from hydrogen bonding and van der Waals forces. Site marker displacement studies confirmed selective binding at Sudlow site I (subdomain IIA). 3D fluorescence spectroscopy revealed conformational changes in both tertiary and secondary structures of BSA upon RSM binding, consistent with allosteric modulation.These experimental results were further supported by molecular docking, which showed a favorable binding energy (–7.3 kcal mol^{-1}) and stabilizing interactions involving SER428 (hydrogen bonding), HIE145 (π–π stacking), and ARG458 (π–cation interaction) within the binding site.

Overall, the findings confirm that RSM binds specifically and strongly to BSA, inducing conformational changes through a static, electrostatically driven mechanism.

4.2 Future Plans

In the future, I aim to structurally modify RSM to minimize or prevent conformational changes in the target protein upon binding, thereby preserving its native structure. This will allow a more precise investigation of the binding mechanism, including interaction kinetics and specificity. Following structural optimization, further studies will focus on evaluating the probe's potential in real-time bioimaging and other biomedical applications under physiologically relevant conditions.

CHAPTER-5
REFERENCES

5.1 References

1. Lakowicz, J.R. (ed.) (2006) *Principles of Fluorescence Spectroscopy*, Springer US, Boston, MA.
2. Tellinghuisen, J. (1987) The Franck-Condon Principle, pp. 149–156.
3. Kasha, M. (1950) Characterization of electronic transitions in complex molecules. *Discuss Faraday Soc*, **9**, 14.
4. Minoshima, M., Reja, S.I., and Kikuchi, K. (2024) Fluorescence and Phosphorescence Spectroscopy, in *Instrumental Analysis of Coordination Compounds*, Royal Society of Chemistry, pp. 259–278.
5. Eng, J., and Penfold, T.J. (2020) Understanding and Designing Thermally Activated Delayed Fluorescence Emitters: Beyond the Energy Gap Approximation. *The Chemical Record*, **20** (8), 831–856.
6. Parker, C.A., Hatchard, C.G., and Joyce, T.A. (1964) P-type delayed fluorescence from ionic species and aromatic hydrocarbons. *J Mol Spectrosc*, **14** (1–4), 311–319.
7. Xie, Y., Li, J., Mei, L., Luo, S., Zhang, T., Zhang, X.-H., and Chen, X.-K. (2024) Mechanisms of TADF/Phosphorescence-Sensitized Fluorescence in OLED Emissive Layers and Their Impacts on Device Performances: A Theoretical Insight. *The Journal of Physical Chemistry C*, **128** (46), 19767–19776.
8. Kim, N., Kang, M.J., Lee, H.J., Park, J.Y., Kwak, H., Park, C.Y., Ahn, H.J., Kim, J., Baek, J., Kim, H.Y., Park, S., Cho, M.J., Choi, D.H., and Kim, T.G. (2024) Enhancing Narrowband Blue TADF OLED Performance with Adamantane Group-Integrated Spatially Hindered 1,3-Bis(N-Carbazolyl)Benzene-Based Host. *Adv Funct Mater*, **34** (48).

9. Shi, W., Li, Y., Zhang, Z., Tan, Z., and Yang, S. (2024) Synthesis and characterization of machine learning designed TADF molecules. *Heliyon*, **10** (23), e40750.
10. Andrienko, D.A., and Boyd, I.D. (2016) Master Equation Study of Vibrational and Rotational Relaxations of Oxygen. *J Thermophys Heat Trans*, **30** (3), 533–552.
11. Shi, L., Xie, X., and Troisi, A. (2022) Rapid calculation of internal conversion and intersystem crossing rate for organic materials discovery. *J Chem Phys*, **157** (13).
12. Noda, H., Nakanotani, H., and Adachi, C. (2018) Excited state engineering for efficient reverse intersystem crossing. *Sci Adv*, **4** (6).
13. Shivaleela, B., Shivraj, G.G., Mayadevi, K., Mahantesh, B., and Hanagodimath, S.M. (2022) Effect of solvent on fluorescence and absorption spectra of fluorescent coumarin derivative: Estimation of ground and excited state dipole moments. *Mater Today Proc*, **68**, 564–572.
14. Huo, X., Shen, H., Liu, R., and Shao, J. (2021) Solvent Effects on Fluorescence Properties of Carbon Dots: Implications for Multicolor Imaging. *ACS Omega*, **6** (40), 26499–26508.
15. Haidekker, M.A., Brady, T.P., Lichlyter, D., and Theodorakis, E.A. (2005) Effects of solvent polarity and solvent viscosity on the fluorescent properties of molecular rotors and related probes. *Bioorg Chem*, **33** (6), 415–425.
16. Bixon, M., and Jortner, J. (1993) Solvent relaxation dynamics and electron transfer. *Chem Phys*, **176** (2–3), 467–481.
17. Zhao, J., Zeng, Y., and Zheng, X. (2022) Conformational Flexibility-Controlled Piezochromic Behavior of Organic Fluorophores. *Chemistry of Materials*, **34** (23), 10711–10720.
18. Iimori (飯森俊文), T., Ishikawa (石川拓), T., Torii (鳥井悠人), Y., Tamaya (玉谷穂菜美), H., Nakano (中野英之), H., and Kanno (菅野眞生), M. (2020) Effect of rigidity of microenvironment on fluorescence of 7,7,8,8-tetracyanoquinodimethane (TCNQ). *Chem Phys Lett*, **738**, 136912.
19. Misra, R., and Bhattacharyya, S.P. (2018) *Intramolecular Charge Transfer*, Wiley.
20. Jankowska, J., and Sobolewski, A.L. (2021) Modern Theoretical Approaches to Modeling the Excited-State Intramolecular Proton Transfer: An Overview. *Molecules*, **26** (17), 5140.

21. Zhou, P., and Han, K. (2018) Unraveling the Detailed Mechanism of Excited-State Proton Transfer. *Acc Chem Res*, **51** (7), 1681–1690.
22. Liao, R., Wang, X., Peng, L., Sun, H., and Huang, W. (2021) Achieving Organic Smart Fluorophores by Controlling the Balance between Intermolecular Interactions and External Stimuli. *ACS Appl Mater Interfaces*, **13** (23), 27491–27499.
23. Brokmann, X., Coolen, L., Dahan, M., and Hermier, J.P. (2004) Measurement of the Radiative and Nonradiative Decay Rates of Single CdSe Nanocrystals through a Controlled Modification of their Spontaneous Emission. *Phys Rev Lett*, **93** (10), 107403.
24. Tanwar, A.S., Parui, R., Garai, R., Chanu, M.A., and Iyer, P.K. (2022) Dual "Static and Dynamic" Fluorescence Quenching Mechanisms Based Detection of TNT via a Cationic Conjugated Polymer. *ACS Measurement Science Au*, **2** (1), 23–30.
25. Żamojć, K., Bylińska, I., Wiczk, W., and Chmurzyński, L. (2021) Fluorescence Quenching Studies on the Interactions between Chosen Fluoroquinolones and Selected Stable TEMPO and PROXYL Nitroxides. *Int J Mol Sci*, **22** (2), 885.
26. Mandal, B., Joy, C., Semenov, A., and Babikov, D. (2022) Mixed Quantum/Classical Theory for Collisional Quenching of PAHs in the Interstellar Media. *ACS Earth Space Chem*, **6** (3), 521–529.
27. Gehlen, M.H. (2020) The centenary of the Stern-Volmer equation of fluorescence quenching: From the single line plot to the SV quenching map. *Journal of Photochemistry and Photobiology C: Photochemistry Reviews*, **42**, 100338.
28. Pan, B., Liu, Y., Xiao, D., Wu, F., Wu, M., Zhang, D., and Xing, B. (2012) Quantitative identification of dynamic and static quenching of ofloxacin by dissolved organic matter using temperature-dependent kinetic approach. *Environmental Pollution*, **161**, 192–198.
29. Genovese, D., Cingolani, M., Rampazzo, E., Prodi, L., and Zaccheroni, N. (2021) Static quenching upon adduct formation: a treatment without shortcuts and approximations. *Chem Soc Rev*, **50** (15), 8414–8427.
30. Raczuk, E., Dmochowska, B., Samaszko-Fiertek, J., and Madaj, J. (2022) Different Schiff Bases—Structure, Importance and Classification. *Molecules*, **27** (3), 787.
31. Oladipo, S.D., Luckay, R.C., Olofinsan, K.A., Obakachi, V.A., Zamisa, S.J., Adeleke, A.A., Badeji, A.A., Ogundare, S.A., and George, B.P. (2024) Antidiabetes and antioxidant potential of Schiff bases derived from 2-naphthaldehye and substituted aromatic amines: Synthesis, crystal structure, Hirshfeld surface analysis, computational, and invitro studies. *Heliyon*, **10** (1), e23174.

32. Wei, L., Tan, W., Zhang, J., Mi, Y., Dong, F., Li, Q., and Guo, Z. (2019) Synthesis, Characterization, and Antifungal Activity of Schiff Bases of Inulin Bearing Pyridine ring. *Polymers (Basel)*, **11** (2), 371.
33. Matela, G. (2020) Schiff Bases and Complexes: A Review on Anti-Cancer Activity. *Anticancer Agents Med Chem*, **20** (16), 1908–1917.
34. Sedgwick, A.C., Wu, L., Han, H.-H., Bull, S.D., He, X.-P., James, T.D., Sessler, J.L., Tang, B.Z., Tian, H., and Yoon, J. (2018) Excited-state intramolecular proton-transfer (ESIPT) based fluorescence sensors and imaging agents. *Chem Soc Rev*, **47** (23), 8842–8880.
35. Liu, K., Zhang, J., Shi, Q., Ding, L., Liu, T., and Fang, Y. (2023) Precise Manipulation of Excited-State Intramolecular Proton Transfer via Incorporating Charge Transfer toward High-Performance Film-Based Fluorescence Sensing. *J Am Chem Soc*, **145** (13), 7408–7415.
36. Zhang, Q., Yang, L., Han, Y., Wang, Z., Li, H., Sun, S., and Xu, Y. (2022) A pH-sensitive ESIPT molecule with aggregation-induced emission and tunable solid-state fluorescence multicolor for anti-counterfeiting and food freshness detection. *Chemical Engineering Journal*, **428**, 130986.
37. Liu, S., Wang, K., Ke, S., Chen, M., Qian, X., Qin, X., Yin, L., Fan, Q., and Qian, Y. (2024) Organic high-temperature sensing films based on ESIPT material. *Sens Actuators A Phys*, **377**, 115757.
38. Bose, D., and Girigoswami, A. (2025) Excited-State Proton Transfer for Biomarker Detection. *Photochem*, **5** (1), 2.
39. Saravanan, K., Srinivasan, N., Thanikachalam, V., and Jayabharathi, J. (2011) Synthesis and Photophysics of Some Novel Imidazole Derivatives Used as Sensitive Fluorescent Chemisensors. *J Fluoresc*, **21** (1), 65–80.
40. Zhang, C., Li, L., Wu, H., Liu, Z., Li, J., Zhang, G., Wen, G., Shuang, S., Dong, C., and Choi, M.M.F. (2013) Synthesis and photophysical studies of oxazole rings containing compounds as electron accepting units. *Spectrochim Acta A Mol Biomol Spectrosc*, **102**, 256–262.
41. Saleh, A., Saleh, M., and Chemistry, C. (2022) Synthesis of heterocyclic compounds by cyclization of Schiff bases prepared from capric acid hydrazide and study of biological activity. *Egypt J Chem*, **0** (0), 0–0.

42. Kagatikar, S., and Sunil, D. (2021) Schiff Bases and Their Complexes in Organic Light Emitting Diode Application. *J Electron Mater*, **50** (12), 6708–6723.
43. Adamczyk, O., Szota, M., Rakowski, K., Prochownik, M., Doveiko, D., Chen, Y., and Jachimska, B. (2023) Bovine Serum Albumin as a Platform for Designing Biologically Active Nanocarriers—Experimental and Computational Studies. *Int J Mol Sci*, **25** (1), 37.
44. (2023) Selective Binding of Bovine Serum Albumin (BSA): A Comprehensive Review. *Biointerface Res Appl Chem*, **13** (6), 555.
45. Akal, C. (2017) Benefits of Whey Proteins on Human Health, in *Dairy in Human Health and Disease Across the Lifespan*, Elsevier, pp. 363–372.
46. Swinehart, D.F. (1962) The Beer-Lambert Law. *J Chem Educ*, **39** (7), 333.